

Design and Development of a Nano-positioning Actuator

*Submitted in partial fulfillment of the
requirements for the award of degree of*

**BACHELOR OF TECHNOLOGY
IN
MECHANICAL ENGINEERING**

Submitted by:
Shrey Shah (19BME134)



**MECHANICAL ENGINEERING DEPARTMENT
INSTITUTE OF TECHNOLOGY
NIRMA UNIVERSITY
Year: 2019-23**

Declaration

This is to certify that

- The thesis comprises my original work towards the degree of Bachelor of Technology in Mechanical Engineering at Nirma University and has not been submitted elsewhere for degree.
- Due acknowledgement has been made in the text to all other material used.

Signature of student

Name: Shrey Shah

Roll No: 19BME134

Undertaking for Originality of the Work

I, Shrey Dharmendra Shah (19BME134) give undertaking that the Major Project entitled “Design and Development of a Nano-positioning Actuator” submitted by me, towards the partial fulfillment of the requirements for the degree of Bachelor of Technology in Mechanical Engineering of Nirma University, Ahmedabad, is the original work carried out by me. I give assurance that no attempt of plagiarism has been made. We understand that in the event of any similarity found subsequently with any published work or any dissertation work elsewhere; it will result in severe disciplinary action.

Signature of Student:

Date:

Place: Ahmedabad

Endorsed by:

Dr. Mihir Chauhan

Assistant Professor

Department of Mechanical Engineering,
Nirma University,
Ahmedabad.

Signature of Guide:

Plagiarism Report

Report2

ORIGINALITY REPORT

9%
SIMILARITY INDEX **8%**
INTERNET SOURCES **2%**
PUBLICATIONS **7%**
STUDENT PAPERS

PRIMARY SOURCES

1	Submitted to Institute of Technology, Nirma University Student Paper	2%
2	ncttm.edu.np Internet Source	1 %
3	esmats.eu Internet Source	1 %
4	lugm.org Internet Source	<1 %
5	ntrs.nasa.gov Internet Source	<1 %
6	Submitted to Columbia University Student Paper	<1 %
7	Submitted to International School of Helsingborg Student Paper	<1 %
8	docplayer.net Internet Source	<1 %
9	www.ece.ucf.edu	

Certificate

भारत सरकार
अंतरिक्ष विभाग
जंतरिक्ष उपयोग केन्द्र
आंबावाडी विस्तार डाक घर,
अहमदाबाद-380 015. (भारत)
फ़ोनमाय : +91-79-26913050, 26913060
वेबसाईट : www.sac.isro.gov.in/www.sac.gov.in



Government of India
Department of Space
SPACE APPLICATIONS CENTRE
Ambawadi Vistar P.O.
Ahmedabad - 380 015. (INDIA)
Telephone : +91-79-26913050, 26913060
website : www.sac.isro.gov.in/www.sac.gov.in

Scientific Research and Training Division (SRTD)
Research, Outreach and Training Coordination Group (RTCG)
Management and Information Systems Area (MISA)

CERTIFICATE

This is to certify that **Mr. Shrey Shah**, a student of B. Tech (Mechanical Engineering) of Nirma University, Ahmedabad, Gujarat has completed a 16-week (16 January-2023 to 16 May-2023) project on "**Design and Development of Hexapod System**" under the supervision of Sri. Sahil Patel, Sci/Engr-SD, MESA-OPMG-OMDD, Space Applications Centre (ISRO), Ahmedabad. The research work was carried out through Scientific Research and Training Division (SRTD) of Space Applications Centre, Ahmedabad.

(Signature)
श्री. सौरभ व्यास / Dr. S.P. Vyas
इन विभाग के अनुबचन एवं परिवेत्ता व्यास
इन विभाग के अनुबचन एवं परिवेत्ता व्यास/
प्रबन्ध विभाग से संबंधित
प्रबन्ध विभाग के इयासी
Space Applications Centre (ISRO)
अंतरिक्ष विभाग / Department of Space
भारत सरकार / Government of India
अहमदाबाद / Ahmedabad - 380015

TO WHOMSOEVER IT MAY CONCERN

This is to certify that, Mr. Shrey Dharmendra Shah, a student of B.Tech (Mechanical engineering), VIIIth Semester of, Institute of Technology, Nirma University has satisfactorily completed the project report titled “Design and Development of a Nano-positioning Actuator”.

Date:

University Guide:

Dr. Mihir Chauhan
Assistant Professor
Department of Mechanical Engineering,
Institute of Technology
Nirma University, Ahmedabad

Industry Guide:

Shri. Sahil Patel
Scientist/Engr. - SD
OMDD/OPMG/MESA
Space Applications Centre
ISRO, Ahmedabad

Department Head:

Dr. K.M. Patel
Head and Professor,
Department of Mechanical Engineering,
Institute of Technology
Nirma University, Ahmedabad

Approval Sheet

The Project entitled "**Design and Development of a Nano-positioning Actuator**" by **Shrey Shah (19BME134)** is approved for the degree of Bachelor of Technology in Mechanical Engineering.

Examiners

Date: _____

Place: _____

Acknowledgment

This report is based on the internship program as the partial fulfillment of course objective and Requirements for the degree of Bachelor of Technology in Mechanical Engineering. I perceive it was the best way to experience the working environment, procedures, techniques, and Implementation of academics in the mechanical industry/organization. First, I would like to thank the Institute of Technology, Nirma University (ITNU), for including and organizing this internship program in the course. I had an opportunity for the internship at Space Application Centre (SAC)-ISRO; for me, which is the big milestone in my career development. I would like to thank Prof. Shruti Bhatt for providing me the four months of internship program enriching me with valuable practical knowledge regarding the implementation of mechanical design and control systems for a robotic manipulator.

Moreover, it is my radiant sentiment to place on record my deepest gratitude to Dr. S.P.Vyas (Head, Sci./Engr.-SG, MISA/RTCG/SRTD) and Mr. Santosh Tripathi (Sci./Engr.-SF, MISA/RTCG/SRTD) for providing me a chance to work as researcher/trainee at SAC and for giving necessary guidance and arranging all facilities at workplace.

I also would like to express my sincere gratitude towards my industry mentors Mr. Sahil Patel (Sci./Engr.-SD, OMDD/OPMG/MESA), Mr. Naimesh Patel (Head, Sci/Engr-SG, OMDD/OPMG/MESA) and Mr. Shaunak Joshi (Group Director Sci./Engr.-SG, OMDD/OPMG/MESA) for their continuous support and guidance throughout the internship till yet, for keeping a watchful eye on the progress on my work and for always being available when I needed their advice. I am grateful towards my university mentor, Dr. Mihir Chauhan (Assistant Professor, Mechanical department/ITNU) for his valuable comments, inputs efforts and contribution which has been significant in the completion of my internship.

Last but not the least; I couldn't remain still without expressing my sincere thanks to all of my colleagues for their individual coordination, support, help and sincere cooperation during the internship period.

Name: Shrey D Shah

Date:

Place: Ahmedabad

Abstract

An extremely precise positioning mechanism is to be developed for optical positioning of mirrors of a space telescope. According to accommodation of the telescope in launch vehicles, segmented mirrors are employed to fit huge mirrors within. After the unfolding is complete, the secondary mirror must be used to focus light from distant planets and stars with the arrangement of these segmented mirrors being crucial for the quality of the image that results. The six actuators for the six degrees of freedom of these segmented mirrors are positioned behind each individual segment to allow for both fine and coarse placement. Since the full mirror is being segmented into smaller mirrors, for high precision these actuators need to be developed in such a way that the segmented mirrors form a complete mirror after unfolding and positioning.

These actuators are built with commonly found mechanical elements such gears, bearings, camshafts, and ball screws. The motion reduction structure, one of the two erudite sub-assemblies employed in the design, is a well-controlled passive system that smoothly reduces a coarse input given in micrometers to a fine output received in nanometers with no backlash. Additionally, coarse-drive coupling, which contains projecting pins on each shaft, satisfy the need for obtaining fine motion independently. When these shafts are engaged, combined motion is produced; however, when these shafts are separated, only fine motion is acquired.

To maximize the reduction ratio, the motion reduction flexure is optimized while maintaining the factor of safety under control. These actuators provide both coarse and fine motion with a precision of less than < 10 nanometers over a range of 5 millimeters. Further employing control Mechanism for a complete feedback control, the coarse and fine motion was controlled to reach the desired position. 2 Actuators were assembled as bipod structures for 2 DOF control. Finally moving on to the hexapod assembly and control, this study describes the design strategy, computations, and control algorithms and optimization techniques from developing an actuator to entire hexapod with 6 DOF.

Table of Contents

1. Introduction.....	6
1.1. About the Project	7
1.2. Actuator requirements and availability	8
2. Structural Overview	8
2.1. Actuator Sub-Assemblies.....	9
2.1.1. Gear-Motor Assembly	9
2.1.2. Coarse-Drive Coupling.....	9
2.1.3. Ballscrew coupling	9
2.1.4. Torsional Stabilizer.....	9
2.1.5. Disk Brake	9
2.2. Gear Selection	10
2.3. Motor Selection.....	11
2.4. Sensor Selection	11
2.5. Gear Pass Calculations	12
2.6. Motion Reduction Structure (MRS) Modeling.....	13
2.6.1. Parametric Variation.....	14
2.7. Disk Brake Design	19
2.8. Modelling of other Actuator parts.....	20
3. Integrated testing of a Single Actuator System.....	21
3.1. Drive electronics	22
3.2. Coarse motion testing.....	23
3.3. Fine Motion Testing	25
3.4. Combined Theoretical movement.....	26
3.5. Load Handling Capacity.....	27
3.6. Attaching Disk Brake.....	28
3.7. Coarse Control Algorithm.....	29
3.8. Fine Control Mechanism	32
3.9. Combined Control Mechanism	34
3.9.1. Mathematical verification	35
3.10. Basic GUI design for controlling Actuators	36
4. Addressing discrepancies and ensuring consistency.....	37
4.1. External Repeatability Testing	39
4.2. Mass experimentation	40
4.3. Stability check.....	42
4.4. Relative Repeatability.....	44

5.	Multi-Actuator Integration System and Testing.....	45
5.1.	Integrated Drive Electronics	45
5.2.	Testing of 6 Assembled Actuators.....	47
5.3.	Load Handling of 6 Actuators.....	49
6.	Bipod Integration and testing	50
6.1.	Z-axis Motion Control Demonstration	50
6.1.1.	Sinusoidal verification	52
6.2.	Correlation of Legs of the Bipod.....	53
6.3.	Control Mechanism for Bipod Assembly	55
6.3.1.	Independent Location Hunting.....	56
6.3.2.	Dependent Location Hunting.....	58
7.	Stewart Platform (Hexapod Assembly)	60
7.1.	Assembly of Hexapod.....	61
7.2.	Inverse Kinematics of the Hexapod.....	63
7.3.	Z-control of Hexapod platform.....	65
7.4.	Bonding of Dummy Mirror	65
7.5.	Rx and Ry control	65
8.	Summary and Conclusion	66
8.1.	Future work	66
9.	References.....	67

List of Figures

FIGURE 1 WORKING MECHANISM OF THE TELESCOPE	7
FIGURE 2 WORKING MECHANISM OF ACTUATOR.....	10
FIGURE 3 SELECTED MOTOR DIMENSIONS.....	11
FIGURE 4 INITIAL MODEL	14
FIGURE 5 FINAL MODEL.....	14
FIGURE 6 PARAMETER NOTATION.....	15
FIGURE 7 SIMULATIONS OF MRS.....	17
FIGURE 8 EFFECT OF MAJOR ANGLES	18
FIGURE 9 RADIUS VS FORCE OF BRAKING PAD	19
FIGURE 10 DISK PAD MODELING AND SIMULATION.....	19
FIGURE 11 ACTUATOR PARTS	20
FIGURE 12 SINGLE ACTUATOR ASSEMBLY.....	21
FIGURE 13 SINGLE ACTUATOR ASSEMBLY.....	22
FIGURE 14 DRIVE CONNECTIONS	23
FIGURE 15 COARSE MOTION	24
FIGURE 16 INCREMENTAL DIFFERENCE OF LVDT.....	24
FIGURE 17 ERROR MEASURED AT HIGH-SPEED OPERATION.....	24
FIGURE 18 REVOLUTIONS OF ECCENTRIC SHAFT	25
FIGURE 19 MOTOR STEPS VS MOVEMENT (MICRONS).....	26
FIGURE 20 BOX PLOT REMOVING OUTLIERS.....	26
FIGURE 21 VISUALIZATION OF COMBINED MOTION, MOTOR STEPS VS MOVEMENT	27
FIGURE 22 DISENGAGEMENT ERROR BY 1ST MODEL	29
FIGURE 23 DISENGAGEMENT ERROR, IMPROVED BRAKE.....	29
FIGURE 24 COARSE MOTION CONTROL ALGORITHM.....	30
FIGURE 25 LINEAR ADAPTIVE P-CONTROL	31
FIGURE 26 CONVERGENCE OF ADAPTIVE P-CONTROL	31
<i>FIGURE 27 FINE MOTION CONTROL ALGORITHM.....</i>	32
FIGURE 28 CALIBRATION OF FINE MOTION.....	33
FIGURE 29 STEP SIZE PER REVOLUTION	33
FIGURE 30 HUNTING-1 AFTER DISENGAGEMENT	34
FIGURE 31 HUNTING-2	34
FIGURE 32 COMBINED CONTROL ALGORITHM.....	35
FIGURE 33 INITIAL GUI DESIGN	37
FIGURE 34 DUAL DATA ACQUISITION	37
FIGURE 35 MISMATCH OBSERVED B/W INTERNAL AND EXTERNAL MOVEMENT	38
FIGURE 36 INITIAL DISTURBED PLOT	39

FIGURE 37 VERTICAL OFFSET REMOVED	39
FIGURE 38 PHASE SHIFT REMOVED.....	40
FIGURE 39 REPEATABILITY UNDER 10 ITERATIONS.....	41
FIGURE 40 OFFSET GENERATED BY 10 ITERATIONS	41
FIGURE 41 REPEATABILITY UNDER 25 ITERATIONS.....	42
FIGURE 42 OFFSET GENERATED BY 25 ITERATIONS	42
FIGURE 43 STATIC CP ERROR.....	43
FIGURE 44 STATIC CP ERROR: INVAR.....	43
FIGURE 45 REPEATABILITY MAPPED.....	44
FIGURE 46 OFFSET MAPPED	44
FIGURE 47 BLOCK DIAGRAM FOR CENTRAL CONTROLLER UNIT.....	46
FIGURE 48 DRIVE ELECTRONICS SETUP	46
FIGURE 49 TESTING OF 6 ACTUATORS	47
FIGURE 50 ACTUATOR 1	48
FIGURE 51 ACTUATOR 2	48
FIGURE 52 ACTUATOR 3	48
FIGURE 53 ACTUATOR 4	48
FIGURE 54 ACTUATOR 5	48
FIGURE 55 ACTUATOR 6	48
FIGURE 56 BIPOD ASSEMBLIES AND TESTING.....	50
FIGURE 57 BIPOD Z-MOTION (DISENGAGED)	51
FIGURE 58 BIPOD Z-MOTION (ENGAGED).....	51
FIGURE 59 BIPOD MOTION DISTURBANCE.....	52
FIGURE 60 BIPOD CAD MODEL.....	53
FIGURE 61 A2 MOVES A1 IS OBSERVED	54
FIGURE 62 A1 MOVES, A2 IS OBSERVED	54
FIGURE 63 CORRELATION FOR REDUCTION RATIO	55
FIGURE 64 BIPOD INDEPENDENT HUNTING ALGORITHM	57
FIGURE 65 TEST CASES FOR ALGORITHM 1	58
FIGURE 66 BIPOD DEPENDENT HUNTING ALGORITHM	59
FIGURE 67 TEST CASES FOR ALGORITHM 2	60
FIGURE 68 STATIC SIMULATION MODEL.....	61
FIGURE 69 MOVEMENT OF HEXAPOD IN 6 DOF	61
FIGURE 70 HEXAPOD DUMMY MODEL.....	62
FIGURE 71 HEXAPOD FINAL CAD MODEL	62
FIGURE 72 HEXAPOD TEST SETUP WITH DRIVE ELECTRONICS	63

List of Tables

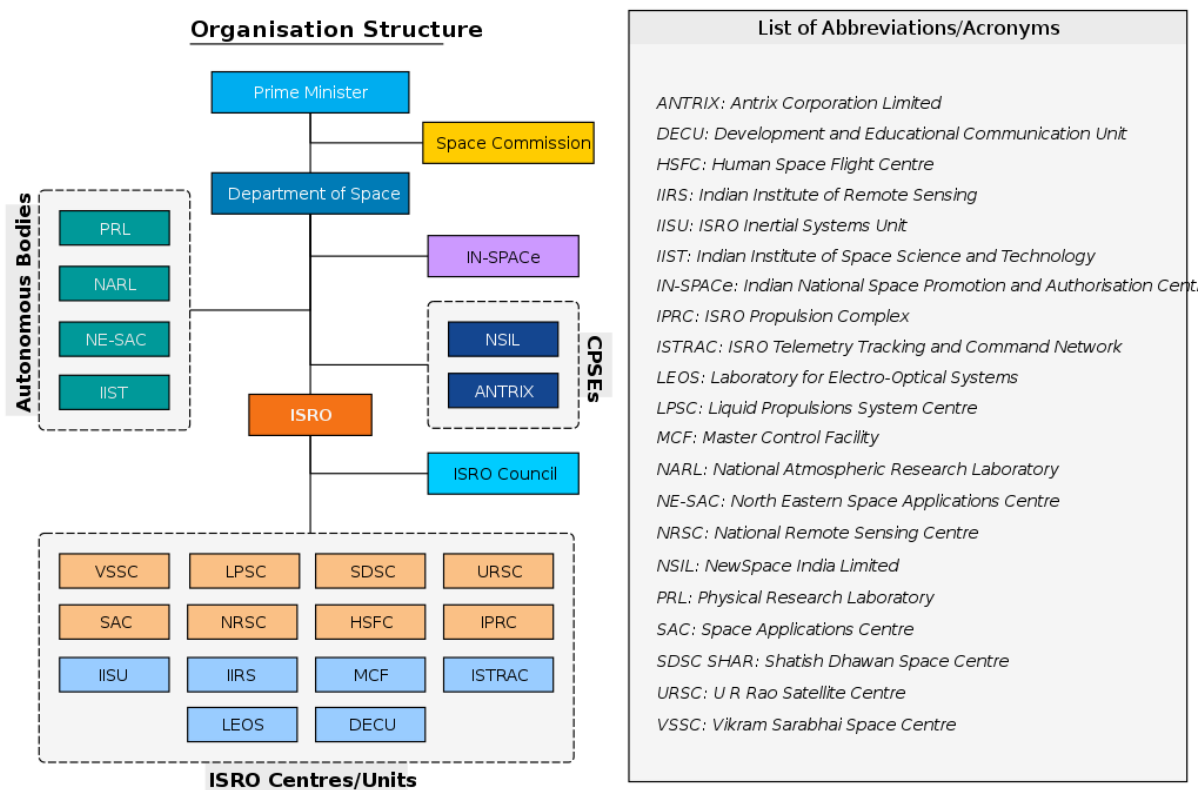
TABLE 1 DESIGN REQUIREMENTS.....	8
TABLE 2 ACTUATOR COMPARISON	8
TABLE 3 GEAR SPECIFICATIONS.....	10
TABLE 4 POWER TRANSMISSION.....	10
TABLE 5 MOTOR REQUIREMENTS	11
TABLE 6 COMPARISON OF SENSORS AVAILABLE.....	12
TABLE 7 GEAR PASS CALCULATIONS	13
TABLE 8 EFFECT OF PARAMETERS	15
TABLE 9 PARAMETRIC VARIATION	15
TABLE 10 MRS TOLERANCE PROVIDED.....	18
TABLE 11 LOAD HANDLING OF SINGLE ACTUATOR	28
TABLE 12 SUMMARY OF MASS EXPERIMENTATION	41
TABLE 13 STEP SIZES OF 6 ACTUATORS	48
TABLE 14 COMPARISON OF 6 ACTUATORS	49
TABLE 15 SLIPPAGE OF 6 ACTUATORS.....	49
TABLE 16 ROTATION MATRIX CALCULATION.....	64
TABLE 17 MAGNITUDE OF MOVEMENT OF ACTUATORS.....	64

1. Introduction

The Indian Space Research Organization (ISRO) is the Government of India's pioneering space investigation office, located in Bengaluru. In order to foster and restrain space innovation in public discourse, while pursuing planetary exploration and space science research, ISRO was established in 1969. ISRO replaced INCOSPAR, which was founded in 1962 by Pt. Jawaharlal Nehru, one of India's most notable prime ministers, and researcher Vikram Sarabhai, who is regarded as one of the key architects of the Indian space program.

The Chairman of ISRO serves as the executive of the Department of Space (DOS), which is also under the direct control of the Prime Minister of India. The organization structure for the same is shown in the image below.

The principal organization in India responsible for duties relating to space-based applications, space exploration, and the advancement of related technology is ISRO. It is one of only six national space agencies in the world with full launch capability, cryogenic engine deployment, extra-terrestrial mission launching, and huge fleets of man-made satellite operations.



1.1. About the Project

Space telescopes are advanced instruments designed to navigate and explore the depths of the universe. By capturing images from distances exceeding a million light years away, they enable us to study the cosmos and gain insights into its origins and evolution. The telescope's primary mirrors are responsible for detecting light rays from distant celestial bodies and reflecting them onto a secondary mirror, which then focuses them onto a detector.

To achieve this, each mirror segment must be placed with extreme precision to ensure the proper assembly of the entire telescope. The mirrors are often arranged into sections and supported by rods, with each segment having six actuators arranged in a tri-bipod assembly. These actuators allow for the controlled translation and rotational movement of each mirror segment about each axis, similar to a Stewart platform used in parallel robotics. By carefully controlling the position and alignment of these mirror segments, space telescopes can provide us with remarkable images and insights into the mysteries of the universe.

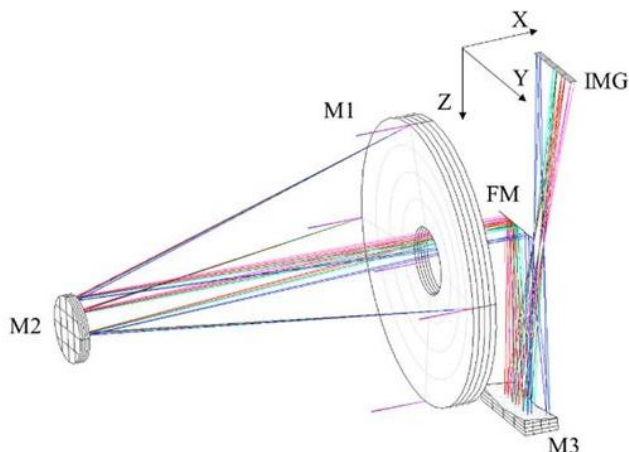


Figure 1 Working Mechanism of the Telescope

To regulate the radius of curvature, an extra actuator is positioned in the center of each section of the mirror. To enable each segmented mirror to function as a uniform entity. An actuator with 2 main types of requirements is needed to support the cause mentioned:

- Accurately position the actuator for them to reflect the light to the secondary mirror
- Fulfil the load criteria during no gravity and 5G.

1.2. Actuator requirements and availability

The positioning requirements were focused primarily for this project. There are plenty of actuators available in the market, a comparison has been made as a part of literature review. The need for custom actuator stems from the need of vacuum compatibility as well has a dual coarse and fine motion when require which most actuators fail to provide. The crucial requirements for the actuators positioning the mirror are given below with the comparison of different types of actuators.

Property needed	Requirement	Capability (fabrication)
Coarse Resolution	< 1 μm	33.33 nm
Coarse range	10 mm	5 mm
Fine Resolution	< 15 nm	\sim 10 nm
Fine range	< 15 μm	14 – 26 μm
Weight	< 400 gm	350 gm
Total Height	< 150 mm	110 mm

Table 1 Design Requirements

Type	Resolution	Range
Hydraulic	Sub micro	High (upto several meters)
Pneumatic	Sub micro	Medium (upto several cms)
Electric	Sub millimetre	High (upto several meters)
Magnetic	Sub millimetre	Low (upto Several mms)
Mechanical	Sub micrometre	High (upto several meters)
Piezoelectric	Nanometre	Low (upto several mms)

Table 2 Actuator Comparison

2. Structural Overview

A stepper motor, a ball screw, bearings, and other conventional mechanical parts make up the mechanism needed to achieve the intended application. In order to lighten and compact the actuator, a single stepper motor is employed for both coarse and fine motion. Additionally, SS was selected for the majority of the actuator's components due to its incredible strength to density ratio. The entire assembly is thought to consist of several major sub-assemblies.

2.1. Actuator Sub-Assemblies

2.1.1. Gear-Motor Assembly

The stepper motor is integrated with a 100:1 planetary gearhead to form a gear motor. The output of the gear motor drives a 3:1 spur gear pass. The meshing gear is mounted on an eccentric shaft with 0.5 mm eccentricity behaving as a cam and follower where the eccentric shaft provides the thrust to the flexure, which is raised by its leg. The motor selected provides enough torque to overcome the stiffness of titanium flexure as well as provide motion. The spur is coupled with a bevel gear to change axis.

2.1.2. Coarse-Drive Coupling

Coarse (combined) motion and fine motion are operated separately when desired. The coupling switches between motions to give higher steps for increased distance and disengages itself for fine steps. The mitter bevel gear pair transmits power, changing directions. The drive shafts act as crown gears with 1 tooth. This results in a total backlash of 300° causing free movement by ‘A’ flexure. A spur gear is attached to the end of drive shaft meshing with the ball screw gear.

2.1.3. Ballscrew coupling

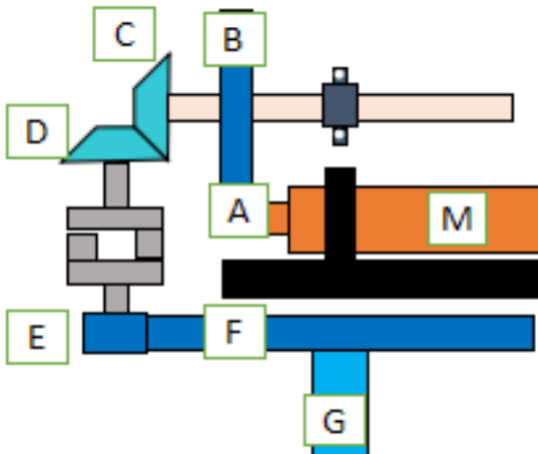
A ballscrew with 1 mm pitch, held by its nut, is connected to the main housing rigidly, providing motion. The spur mesh with a 5:1 ratio transmits power, rotating the screw resulting in a translational movement of the actuator. Bearings are mounted on the ballscrew linking with the main support of the actuator.

2.1.4. Torsional Stabilizer

The ballscrew has a tendency to rotate the actuator support with it. In order to provide only axial motion, the nut of ballscrew is constrained with the main housing. A thin copper shear panel is used resisting the torque applied by the ballscrew and allowing it to translate. As the nut moves up and down, it forms an ‘S’ shape. A pivot is provided to dissipate the radial loading on the ball nut.

2.1.5. Disk Brake

Additional weight can result in back-driving of the actuator. A disk brake was designed and suspended using a cantilever beam below the main actuator structure to prevent back-driving. As a result, the required input torque increases along with reduced risk of back-driving.



M = Stepper Motor
 A = Spur gear on gearhead.
 B = Spur gear on eccentric shaft
 C = Bevel gear on eccentric shaft
 D = Bevel gear on coarse drive shaft
 E = Spur gear on coarse drive shaft
 F = Spur gear ball screw
 G = Ball screw shaft

Figure 2 Working Mechanism of Actuator

2.2. Gear Selection

6 gears continuously reduce the speed and increase the required torque at the same time. Gear A attached to the gearhead of the motor produces a reduction of 100. First reduction by 3 times happens at the pair A and B. Same torque is transmitted to the bevel gear C, being on the same shaft. C and D represent a mitter gear pair with no reduction nor torque waxing. It is utilized for rotating the axis.

In engaged position D transmits same torque to the spur gear E. E and F for another spur gears pair reducing the speed and increasing the torque by a factor of 5. Gears to be Selected should be very compact with the biggest one being F for the ballscrew reduction. Gears A and E are decided to have the same PCD and other properties for shortening fabrications process giving an easy supply of surplus gears. A summary of gear specifications chosen are given below.

Gear notation	PCD	Module	Teeth
A	6	0.4	15
B	18	0.4	45
C	6	0.4	15
D	6	0.4	15
E	6	0.4	15
F	30	0.4	30

Table 3 Gear Specifications

Gear pairs	Gear type	Loses
A - B	Spur to spur	Yes
B - C	Spur to bevel	No
C - D	Bevel to bevel	Yes
D - E	Bevel to Spur (engaged)	Yes
E - F	Spur to Spur	Yes

Table 4 Power Transmission

2.3. Motor Selection

Stepper motors are employed for precise incremental movement when required, with the capacity to provide ample torque for gear actuation, actuator lifting, and support of additional mirror segment loads. To fulfill compact design requirements, strict motor size and weight criteria must be met. Despite rejecting several motors based on size criteria, a suitable motor was eventually selected for the final project and testing, with testing necessitating operation in harsh, high-vibration environments typical of launch conditions. The motor will operate at 1g and undergo load handling testing at 5g. The selected motor provides a input torque of 0.08 Nm with a gearhead reduction of 100 providing 2000 steps per revolution without micro stepping.

Criteria	Requirements
Length	< 45 mm
Diameter	< 20 mm
Torque	> 60 mNm
Degree per step	< 20°
Complementary gearhead	Yes
Gearhead reduction ratio	> 80
Mass	< 20 g
Backlash	< 3°

Table 5 Motor Requirements

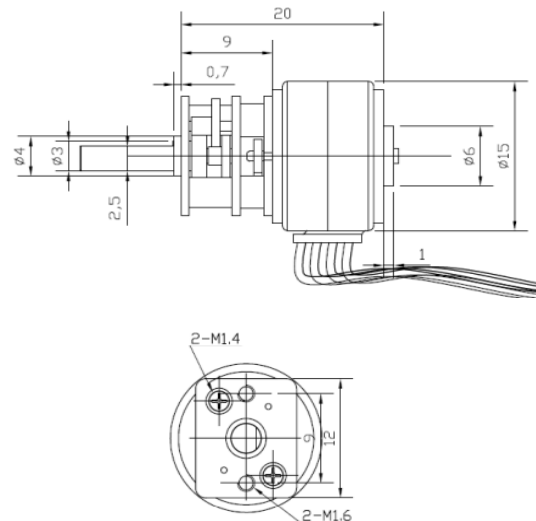


Figure 3 Selected Motor Dimensions

2.4. Sensor Selection

Proximity sensors are available in different categories as per their detection. Some proximity sensors are useful to detect materials; whereas some are useful to detect different environmental conditions. This project will be requiring proximity sensors to sense the physical conditions, environmental conditions will be dealt with by other projects. Proximity Sensors include all sensors that perform non-contact detection in comparison to sensors, such as limit switches, that detect objects by physically contacting them. Proximity Sensors convert information on the movement or presence of an object into an electrical signal. A comparison of available sensors is made and suitable sensors were selected.

Sensor	Range	Resolution	Repeatability	Frequency Response
Inductive	0.5 – 60 mm	0.1 - 2 μm	< $\pm 1 \mu\text{m}$	5 - 100 kHz
Capacitive	0.1 – 20 mm	0.375 - 60 nm	< $\pm 0.1 \text{ nm}$	2 - 8.5 kHz
Ultrasonic	0.3 – 450 cm	100 - 500 μm	< $\pm 1 \text{ mm}$	50 kHz
Infrared	2 – 14 μm	0.5 – 3 μm	< 2 mm	-
Photoelectric	< 1 - 60 mm	0.05 – 1 mm	< 0.05 mm	-

Table 6 Comparison of Sensors available

- a) LVDT - Linear Variable Differential Transformers are the most widely used inductive transducer that converts the linear motion into the electrical signal. The output across secondary of this transformer is the differential thus it is called so. It is very accurate inductive transducer as compared to other inductive transducers.
- b) Capacitance Probe - It is based on an ideal operation of plate-type capacitor. The two plate electrodes are represented by the sensor and the opposing measurement object. If a constant alternating current flows through the sensor capacitor, the amplitude of the alternating voltage is proportional to the distance between the capacitor electrodes. The alternating current is demodulated and output as, for example, an analog signal.

2.5. Gear Pass Calculations

In order to analyze stress and critical junctures in the transmission system, a comprehensive record of torque and forces at each level of transmission is essential. To achieve this, a direct method has been employed for power transmission between each gear pair, accounting for maximum losses and assuming an efficiency of 95% for spur gears. The resulting data is then compiled, providing a summary of input and output values for both torque and forces at each transmission stage. By monitoring and analyzing these values, we can ensure optimal performance and prevent failures or breakdowns within the transmission system.

First pass Gear pair - A and B Input torque = 0.08 Nm Radius of A = 6 mm Radius of B = 18 mm Efficiency = 0.95 Reduction ratio = 3 Force = 13.33 N Force to B = 12.66 N Torque to B = 0.228 Nm	Second Pass Gear pair = C and D Input torque = 0.228 Nm Radius of C = 6 mm Radius of D = 6 mm Efficiency = 0.95 Reduction ratio = 1 Force = 38 N Force to D = 36.1 N Torque to D = 0.216 Nm	
Third Pass Gear pair = E and F Input torque = 0.216 Nm Radius of E = 6 mm Radius of F = 30 mm Efficiency = 0.95 Reduction ratio = 5 Force = 36.1 N Force to F = 34.295 N Torque to F = 1.028 Nm	Fourth Pass Gear pair = F and G (Working as worm gear) Input torque = 1.028 Nm Radius of G = 2 mm Efficiency = 0.95 Reduction ratio = nil Force on G = 514.6 N Torque on G = 1.028 Nm	

Table 7 Gear Pass Calculations

2.6. Motion Reduction Structure (MRS) Modeling

Motion Reduction Structure or MRS is a partly flexible element which reduces the motion provided. It is one of the most crucial elements of the Actuator, governing the fine motion. The range and resolution will be decided by MRS along with the eccentricity of the eccentric shaft. The figure above is simplified version of MRS. The MRS is an A shape with the horizontal bars being the transmission points of the flexure. Vertical movement of the cross beam is given by eccentric shaft connected at the hollow opening. As the eccentric shaft rotates, translational motion is produced at the top. Whilst the cross beam is being deflected, the side holding bars also tend to bend. The up and down motion will result in a sinusoidal curve plotted against the motor steps. Shims under the base can be provided to increase the range of motion by some microns.

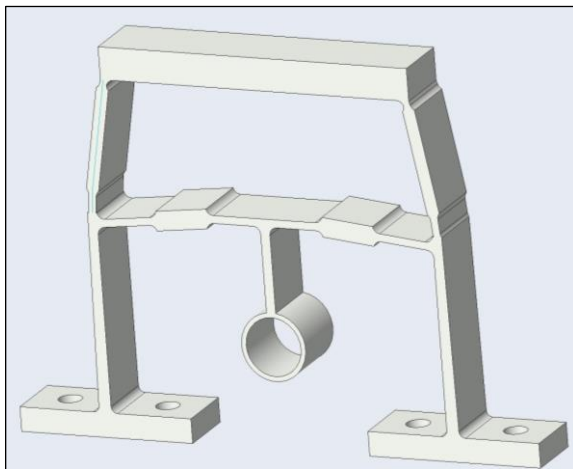


Figure 4 Initial Model

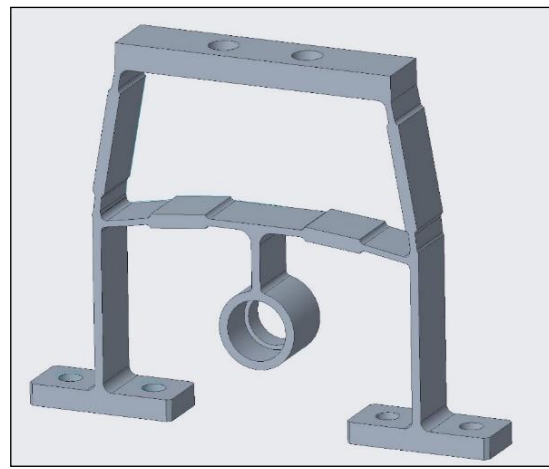


Figure 5 Final Model

2.6.1. Parametric Variation

The model was created and sent to fabrication to compare theoretical calculations with the final product. Testing revealed a reduction ratio of 91.3. The flexure was finalized to be made of titanium due to its high reduction ratio, stiffness, and light weight. It is a single piece part that can be screwed to the base or any other mating part. The most important parameters affecting the reduction ratio are the two angles and thin side thickness, as determined through testing in Creo Parametric. The theoretical analysis was done based on a required reduction ratio of around 70. Varying these parameters produces different reduction ratios, with changes as small as 0.1mm resulting in a 15-point difference. The distances listed in the figure can also be changed to vary the reduction ratio, but they have minimal impact compared to other parameters. Proper care must be taken during fabrication to avoid loss of steps or range in space. The table in the figure shows the important parameters that may govern the reduction ratio of the design, and changing any of these parameters could alter the fine range and resolution undesirably.

Parameter	Notation	Dependency
Thin angle	A	High
Thick angle	B	High
Support angle	C	Low
Thin side thickness	D	Very high
Thick side Thickness	E	Low
Mid-Thickness	F	Very low
Fillets	-	Low

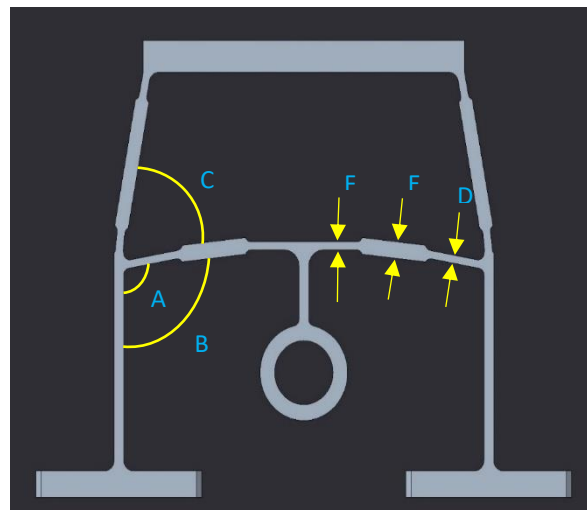


Table 8 Effect of parameters

Figure 6 Parameter Notation

Sr. No.	Thin angle (A)	Thin Thickness (D)	Thick Angle (B)	Thick Thickness (E)	Middle Thickness (F)	Reduction ratio
1.	100	0.8	96	1.6	0.8	72.51
2.	99.5	-	-	-	-	74.43
3.	99	-	-	-	-	80.11
4.	100.5	-	-	-	-	69.25
5.	101	-	-	-	-	65.58
6.	-	0.9	-	-	-	88.88
7.	-	0.7	-	-	-	61
8.	-	-	95.5	-	-	78.20
9.	-	-	95	-	-	86.44
10.	-	-	96.5	-	-	67.32
11.	-	-	97	-	-	62.14
12.	-	-	-	1.7	-	72.75
13.	-	-	-	1.5	-	72.13
14.	-	-	-	-	0.7	71.11
15.	-	-	-	-	0.9	74.57

Table 9 Parametric Variation

The simulation results of one of the many tests is given below showing the variation of stresses generated when a displacement of 0.5 mm is applied to the flexure. A ‘dy’ measure is placed to measure only vertical movement of the top land of ‘A’. The result shows the ideal reduction ratio as $0.5/0.0069 = 72.227$. The stress values at various places are also depicted in it. Since the material to be used is Titanium, the yield stress is very high at 800 Mpa. Following the S-N curve for infinite life, we know that the endurance limit can be found by $S_e = S_{yt}/2$ approximately 400 Mpa, which is well above our current stress produced.

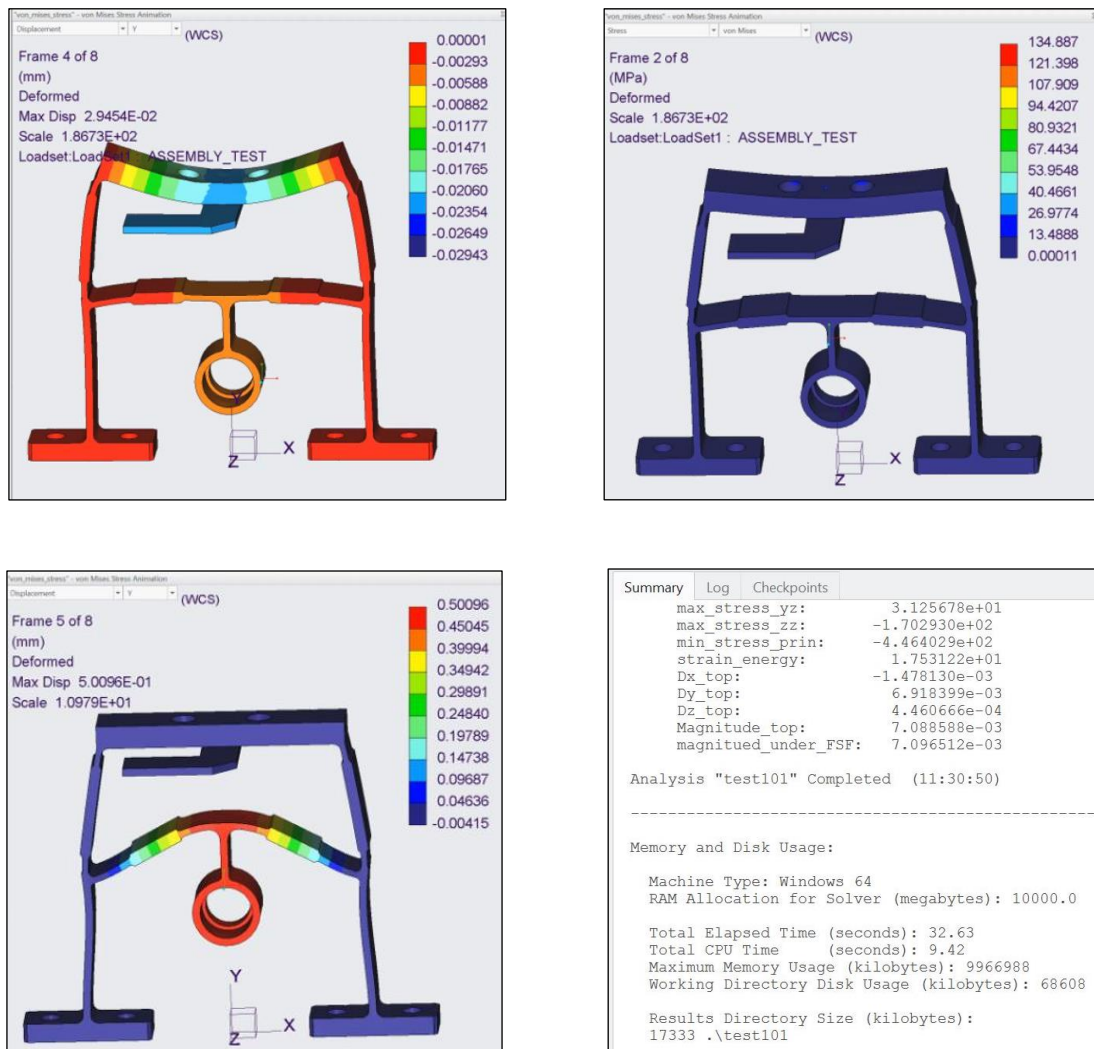


Figure 7 Simulations of MRS

To determine the tolerances, the margins must be higher than the predicted value during the design process. For example, if the thick angle is increased, the reduction ratio is reduced, leading to increased range and resolution. Conversely, if the angle is decreased, the reduction ratio is increased, causing a decrease in range and resolution. When providing tolerances for this angle, it should lean towards the positive side to maintain the desired reduction ratio. The

table below summarizes the finalized tolerances for the critical parameters. After simulating the extreme conditions, the upper and lower limits of the reduction ratio can be found, limiting the possible values of range and resolution. It is important to carefully evaluate these limits to ensure the accuracy and effectiveness of the final product.

- a) Worst case – RR = 74.001
- b) Best case – RR = 59.613

Parameter	Notation	Preferred Higher / Lower	Tolerance
Thin angle	A	Higher	+0.3
Thick angle	B	Higher	+0.3
Support angle	C	Equal	± 0.2
Thin thickness	D	Lower	-0.05
Thick thickness	E	Nominal	± 0.01
Middle thickness	F	Nominal	± 0.01
Middle height	G	Equal	± 0.05

Table 10 MRS Tolerance Provided



Figure 8 Effect of Major angles

2.7. Disk Brake Design

A disk brake prevents back driving of the ballscrew when load exceeding the limit is applied. Although it carries a risk of slippage, the pros outweigh the risk. A disk brake design was selected for easier manufacture and assembly. Based on the gear dimensions, the limits of radius and distance from the center is singled out. Torque required to lift and drop the ball screw is calculated during a load of 575 grams. It could be seen that a negative torque is obtained when moving downwards indicating back driving of the ballscrew. The resultant torque is used as the braking torque needed by the pad to stop the motion. Initial calculations required a 100-micron extension on the pad providing the necessary braking force. The relation between radius and force at fixed distance is given below. Simulation showed promising results and braking. Hence a prototype was modelled and fabricated for testing.

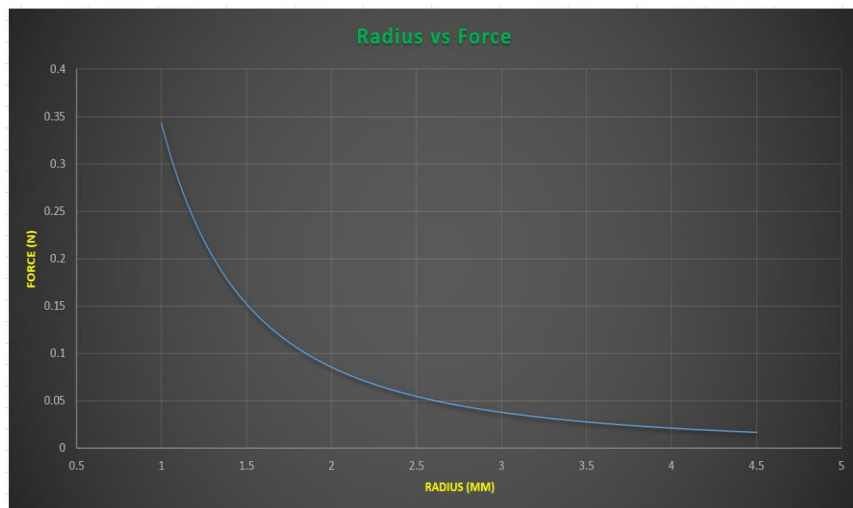


Figure 9 Radius vs Force of braking Pad

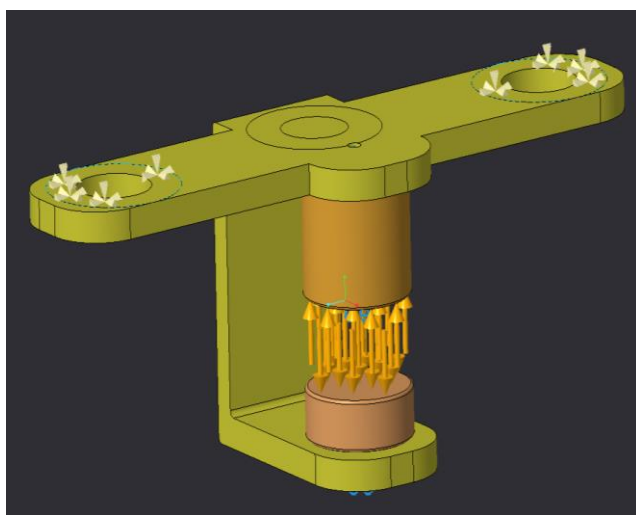
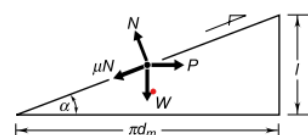
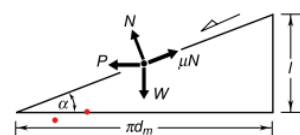


Figure 10 Disk Pad Modeling and simulation

$$P = \frac{W(\tan \phi + \tan \alpha)}{1 - \tan \phi \tan \alpha}$$



$$P = \frac{W(\mu \cos \alpha - \sin \alpha)}{\cos \alpha + \mu \sin \alpha}$$



2.8. Modelling of other Actuator parts

The actuator is not only dependent on the MS and the brake. Parts such as eccentric shaft, the coarse coupling housing, main actuator etc. The critical designs were made and put into fabrication. All in all, around 30 parts were modeled and fabricated for a single actuator. Parts such as bearings, gears and ball screws were ordered from precise industries. 7 sets of all parts with some surplus parts were manufactured to assemble 6 such actuators which will later form a hexapod assembly. An exploded view of the actuator is provided below giving an outline of the assembly. Some parts with secondary importance are also listed below.

- | | | |
|----------------------------------------|------------------------------------|--------------------------|
| 1) Spur gears | 5) Main actuator support structure | 9) Ballscrew support |
| 2) Bevel gears | 6) Fine stage flexure | 10) Main outer support |
| 3) Eccentric camshaft
(fine motion) | 7) Coarse-Drive housing | 11) Shims |
| 4) Bearings | 8) Coarse-Drive shafts | 12) Torsional stabilizer |
| | | 13) Disk brake |

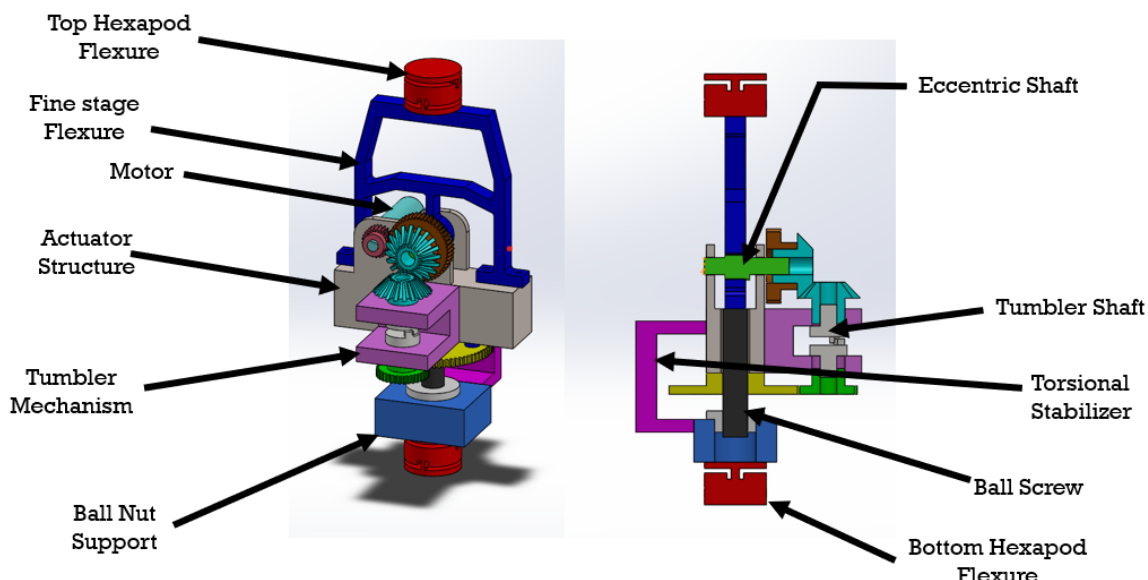


Figure 11 Actuator Parts

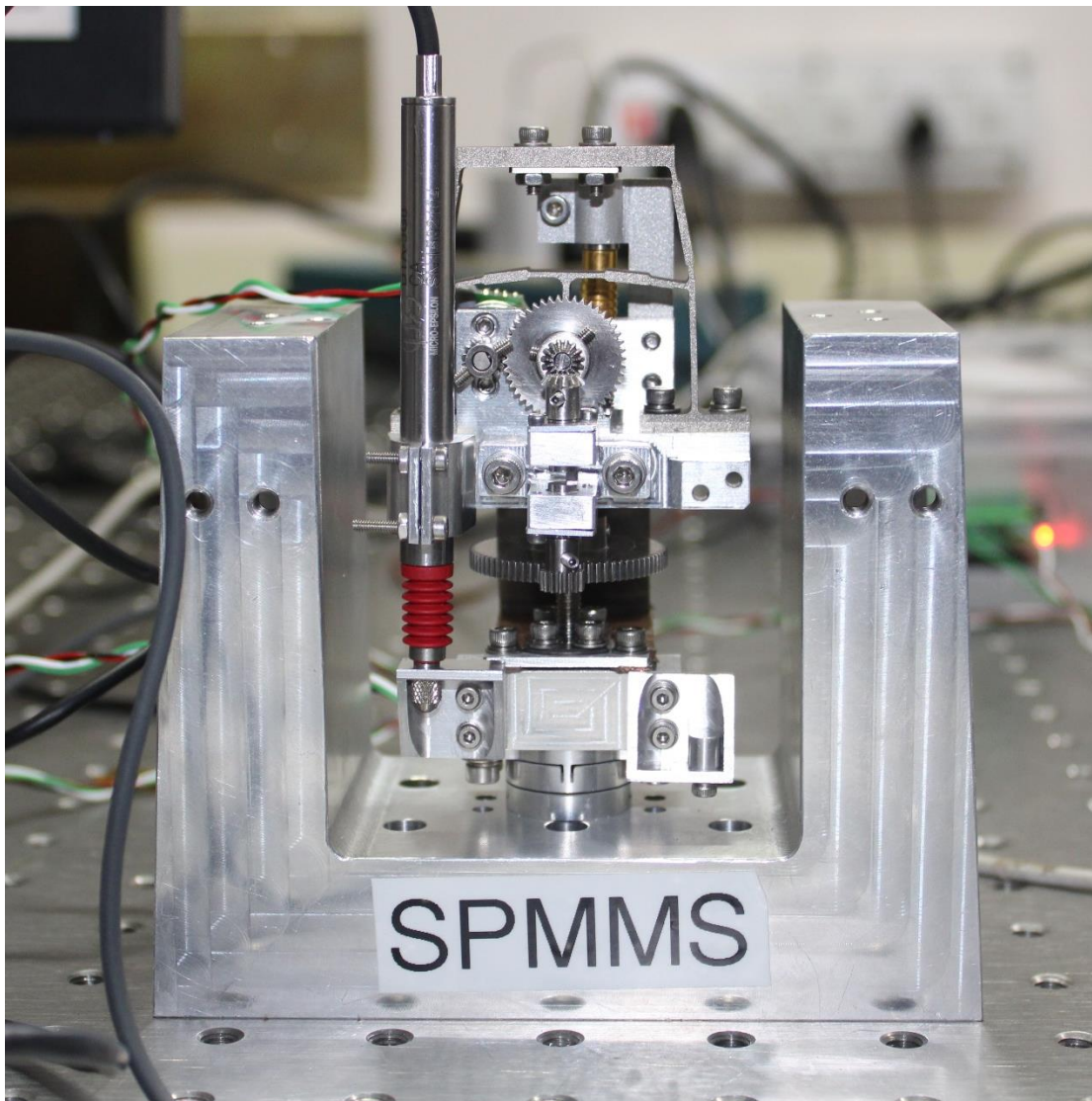


Figure 12 Single Actuator Assembly

3. Integrated testing of a Single Actuator System

After manufacturing an entire actuator was assembled and put to test. Various properties such as the coarse resolution, Fine resolution, smoothness and load handling capacities were considered. After various tests, control action using a closed loop feedback system was incorporated. Such a control system ensures proper movement of the actuator rather than going blind, many inaccuracies in assembly and design may result in needing a feedback system. The algorithms for the control actions were programmed using a raspberry pi in python. Since the system houses 2 different motions, different control algorithms were needed to be developed for each and then one for combining both of them.

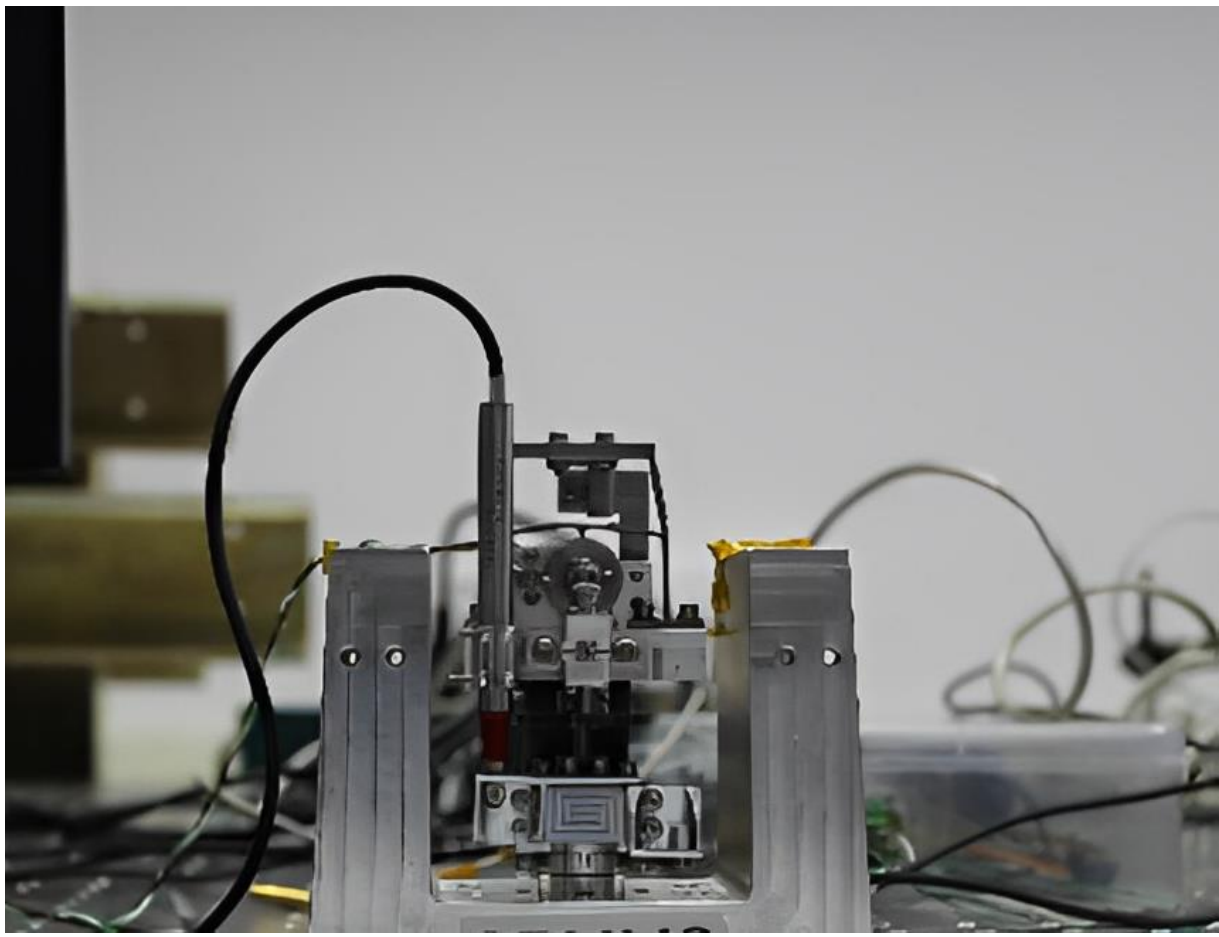


Figure 13 Single Actuator Assembly

3.1. Drive electronics

The actuator that will be designed needs to be driven by stepper motors as stated before. The steppers motors should be able to move at desired speeds and by will. For each actuator 1 motors are required and thus 6 actuators for one mirror. Each motor needs to be controlled by a Driver which also includes micro-stepping if required. The controllers are further powered and governed by either a Raspberry Pi.

The Raspberry Pi is a low cost, credit-card sized computer that plugs into a computer monitor or TV, and uses a standard keyboard and mouse. It is a capable little device that enables people of all ages to explore computing, and to learn how to program in languages like Scratch and Python. It's capable of doing everything you'd expect a desktop computer to do.

The motor is connected to a driver which regulates the pulses and the driver is connected to the Pi to send signals for motion of the motor. The Pi is used for coding in python using the GPIO and RPI modules for stepper motor. A map for connections is shown below.

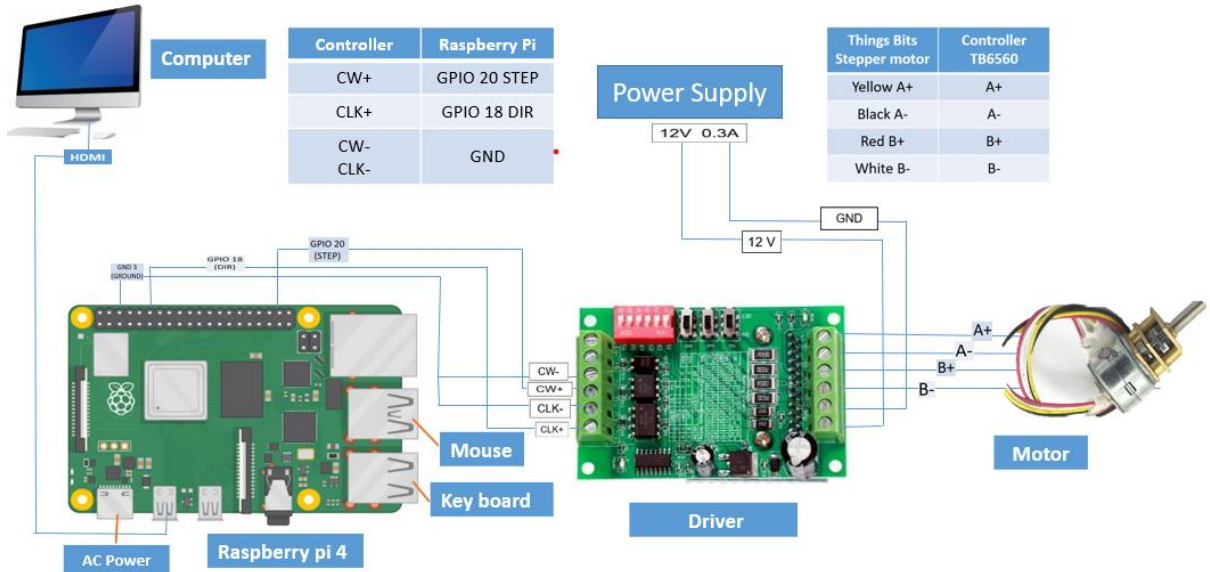


Figure 14 Drive connections

3.2. Coarse motion testing

A vacuum compatible LVDT was brought for testing purposes checking the linear motion of the ballscrew. As the resolution of the sensor is high and theoretical resolution of the ball screw is 33.33 nm, each incremental step data and the overall motion of the actuator was traced. In this test, the fine motion is neglected as it would produce very minute difference during macro-movement. From the graphs, it can be concluded that the motion is fairly straight and predictable under a range of 100 nm. Beyond that, a capacitive probe would be required or hyper precise parts with professional assembly. We can see that over a range of 2400 data points, 500 microns were moved giving a resolution of 208 nm per measurement. At a frequency of 20 Hz, the resolution of measurement becomes 5.4 nm. Error at each reading and each movement is given below.

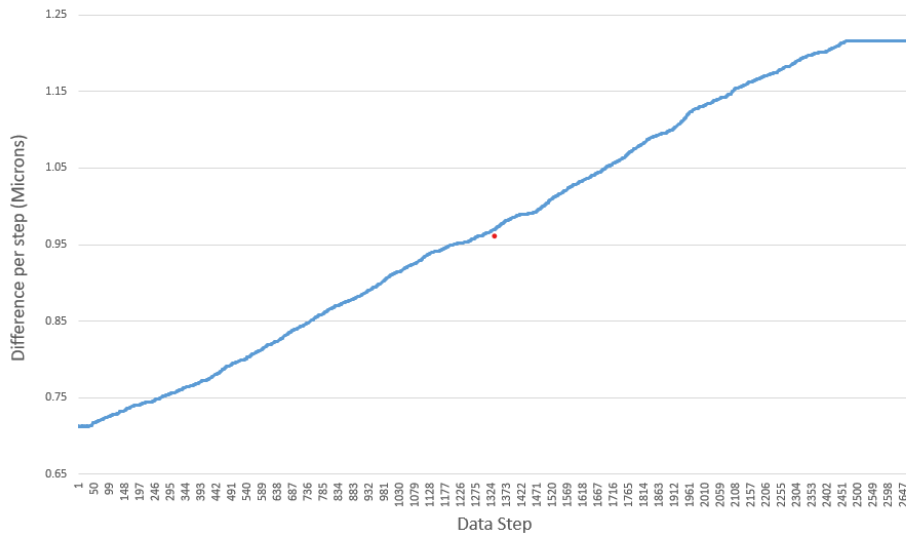


Figure 15 Coarse Motion

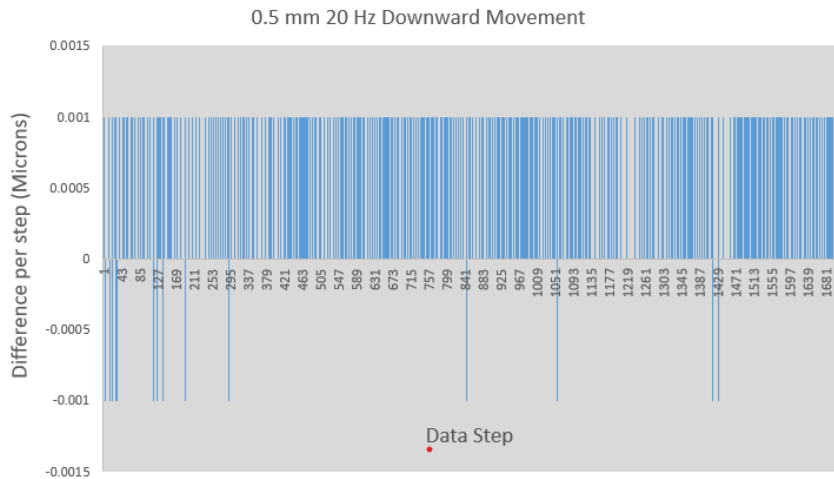


Figure 16 Incremental difference of LVDT



Figure 17 Error measured at high-speed operation

3.3. Fine Motion Testing

Coarse coupler was disengaged and fine motion was tested. As per design the MRS should give a resolution of about 7 nm over a range of \sim 14 microns. It was found that the range and resolution were very close to the designed model, concluding that the MRS was designed seamlessly. A sinusoidal wave generated showed extremities difference of 13.79 microns and using the peak difference to assume a 180° revolution of the camshaft equivalent to 1.5 revolutions of motor. Calculating steps, 3000 motor steps correspond to the range achieved. Simple math proved an average resolution of 4.64 nm. It can be seen from the graphs that there might be some slippage or inaccuracy in motor steps as theoretical 3000 and practical 3003 do not match neither do the steps required to achieve a 180° revolution of the eccentric shaft. A box plot removes the outliers occurred at the peaks of the wave thus maintaining constant increments/decrements.

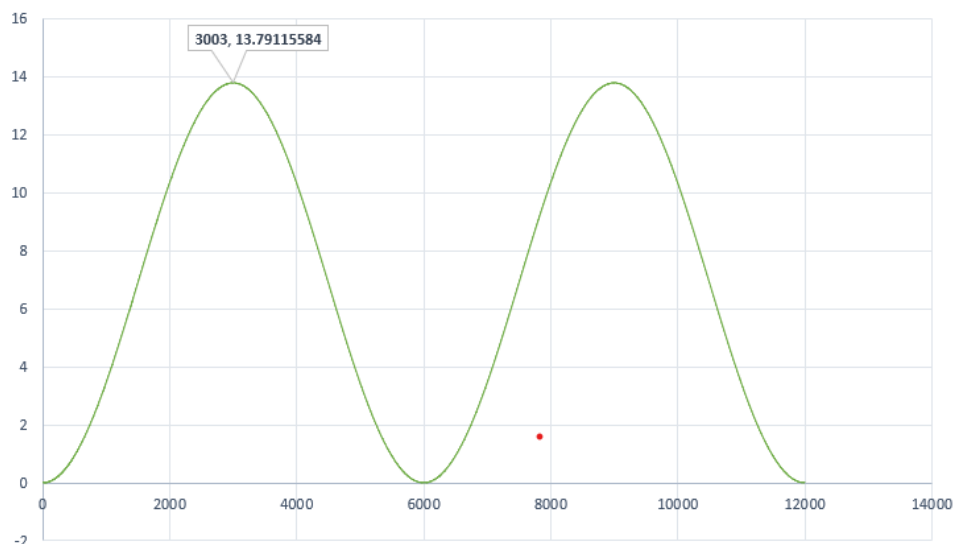


Figure 18 Revolutions of eccentric shaft

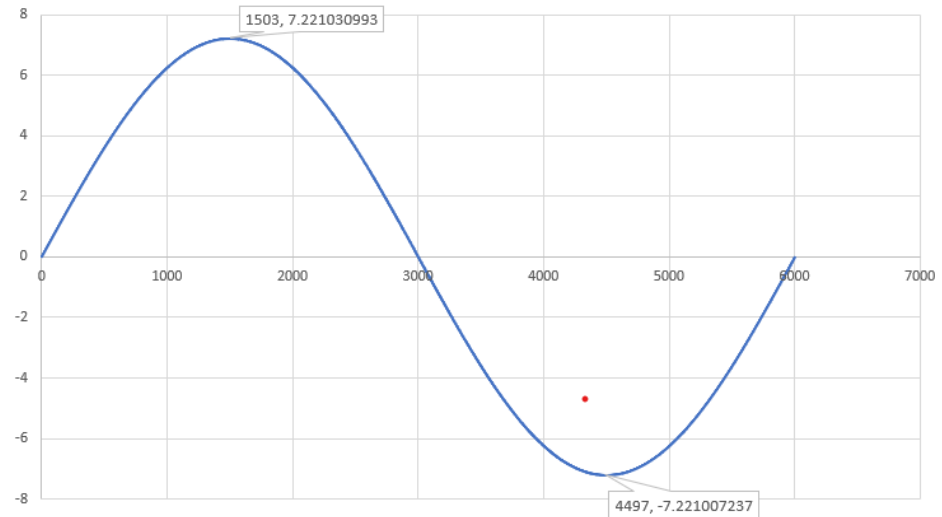


Figure 19 Motor steps vs movement (microns)

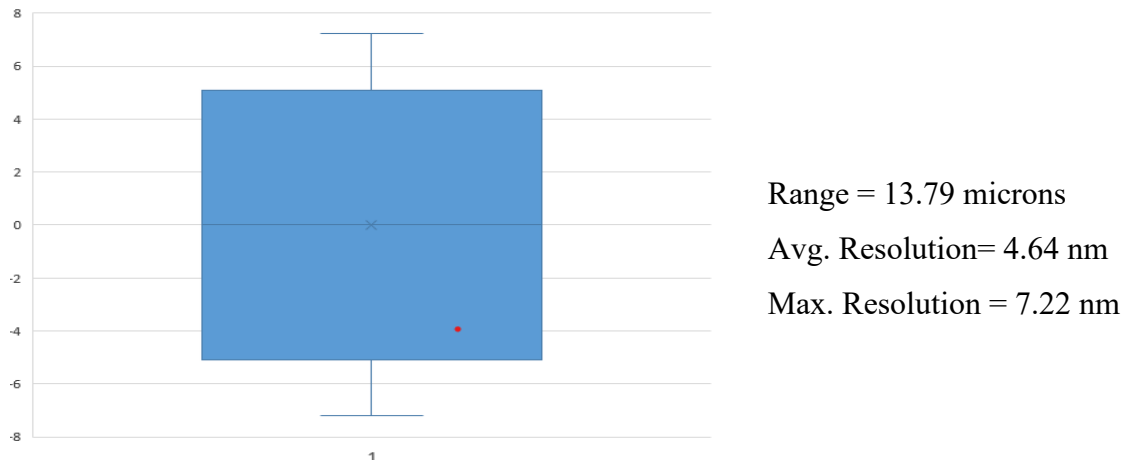


Figure 20 Box plot removing outliers

3.4. Combined Theoretical movement

When the coarse drive is engaged, the combined motion is a result of super position of sinusoidal wave by fine motion and linear line by coarse motion. As a result, countless possibilities may occur when fine tuning rotating motor by a couple of steps. One needs to accurately determine where the fine motion is when engaged and disengaged. A forward movement may not always result in increase in the actuator length. Since we are working in nanometers, it is essential to operate the actuator with complete precision. Control loop algorithms will be devised later to tackle this issue.

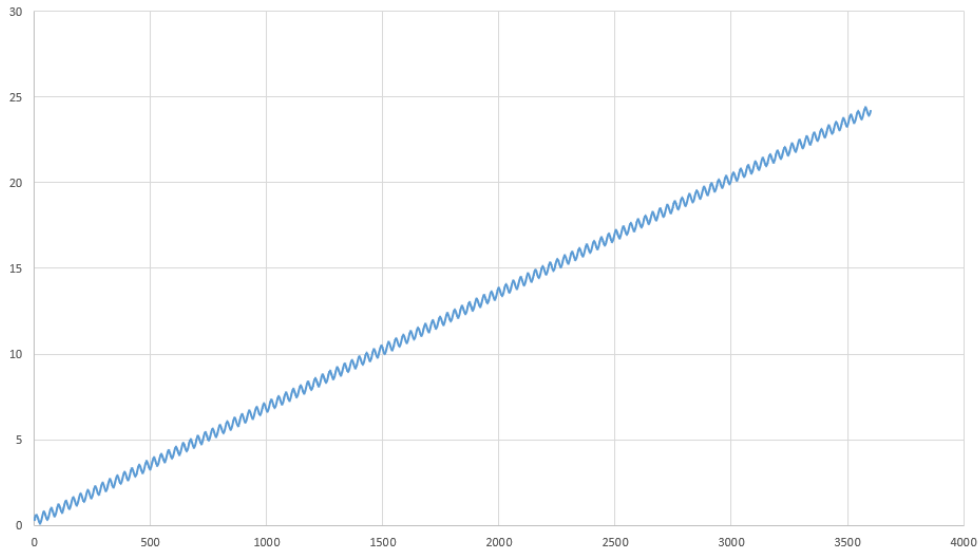


Figure 21 Visualization of combined motion, Motor steps vs Movement

3.5. Load Handling Capacity

A mirror segment of the telescope is expected to weigh ~3 kilos. Assuming each actuator shares the weight equally, a weight of 500 grams needs to be sustained by each individual actuator. Several plates were manufactured each weighing 115 grams. The movement of the actuator is checked along with the range and resolution while increasing the mass on the actuator by 115 grams each time capping at 575 grams. It is crucial that the range and resolution of the actuator are not compromised while maintaining load. Back driving of the ball screw can be verified when the load exceeds the capacity of the ball screw. When this happens the ball screw slips in the backlash provided (270°). When it is engaged again from the other side, the stiffness of titanium of MRS restricts further movement. Although this may be considered an insignificant slip, a movement of 11-12 microns was observed during the slip which is unacceptable to the project. As a result, disk brake was attached and then tested again. A summary of each load test is given below.

Weight	Graph	Range	Avg. Resolution	
-	<p>0 Plate</p> <p>The graph shows a single peak at 897 microns. The x-axis ranges from 1 to 7169 microns, and the y-axis ranges from -10 to 10. The peak is centered around 897 microns.</p> <table border="1"> <tr><td>897</td></tr> </table>	897	13.7628 Microns	4.70 nm
897				
345 g	<p>3 Plates</p> <p>The graph shows a single peak at 729 microns. The x-axis ranges from 1 to 5825 microns, and the y-axis ranges from -10 to 10. The peak is centered around 729 microns.</p> <table border="1"> <tr><td>729</td></tr> </table>	729	14.1818 Microns	4.78 nm
729				
460 g	<p>4 Plates</p> <p>The graph shows a single peak at 728 microns. The x-axis ranges from 1 to 5817 microns, and the y-axis ranges from -10 to 10. The peak is centered around 728 microns.</p> <table border="1"> <tr><td>728</td></tr> </table>	728	13.7456 Microns	4.67 nm
728				
575 g	<p>5 Plates</p> <p>The graph shows a single peak at 730 microns. The x-axis ranges from 1 to 5833 microns, and the y-axis ranges from -10 to 10. The peak is centered around 730 microns.</p> <table border="1"> <tr><td>730</td></tr> </table>	730	14.0867 Microns	4.74 nm
730				

Table 11 Load Handling of Single Actuator

3.6. Attaching Disk Brake

As seen, there is a need for a disk brake to avoid slipping of ballscrew in the backlash provided at the coarse coupling. The fabricated brake was then attached below the main support structure. The first model had an overlap of 100 microns from both ends. It was noted that force necessary to move the ballscrew now was too high. Nonetheless the motor could move it with its working torque of 0.08 Nm. While operating and testing the brake, minor slippage could be seen when the coarse drive is engaged and disengaged. The ballscrew was operated from 0 microns to 2000 microns with an increment of 50 to check the amount of slippage.

At each iteration the disengagement produced a rough error of 24 microns when moving down and 10 microns when lifting the actuator. A remodeling of the brake was necessary and another design with force distribute at both ends of the spur gear was made. This design reduced the force by reducing the overlap to 50 microns resulting in an overall decrease of 150 microns worth of overlap. After reattaching and testing, the disengagement error reduced to 3-4 microns on average which could be compensated by the fine motion with its range of 14 microns or more. Due to gear teeth inaccuracies spikes can been seen at time thought still smaller than 6 microns.

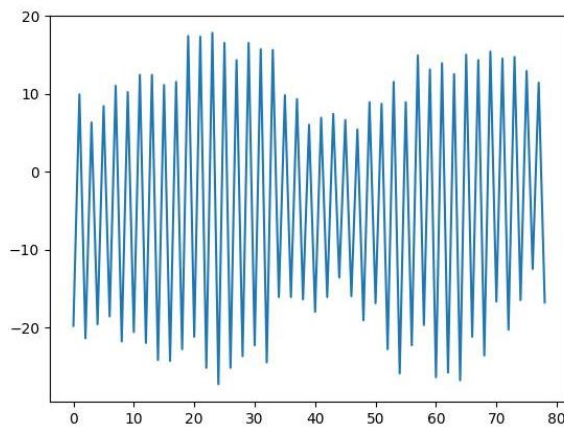


Figure 22 Disengagement Error by 1st Model

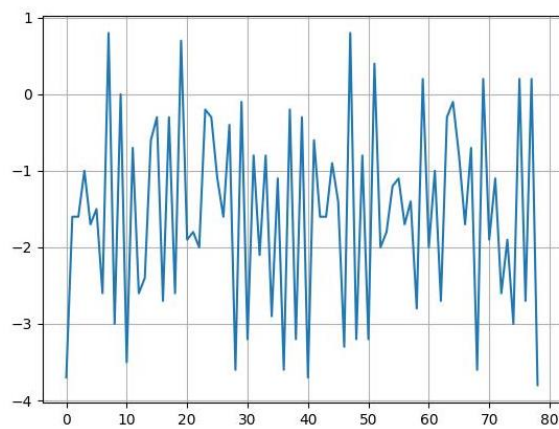


Figure 23 Disengagement Error, Improved brake

3.7. Coarse Control Algorithm

The ballscrew of the actuator handles the quick and coarse movement of the actuator. The control mechanism of the actuator is planned such that, the LVDT is used for coarse control to reach the target position and the Capacitance probe for fine tuning, operated in the backlash of coarse drive mechanism.

PID (proportional-Integral-Derivative) control is the most ideal control suited for an actuators system. The proportional term is based on the current error, or the difference between the desired output and the actual output of the system. It adjusts the input to the system based on the magnitude of the error, in proportion to a pre-defined gain or constant. The integral term takes into account the accumulated error over time and adjusts the input based on the integral of the error. This helps to eliminate any steady-state error in the system. The derivative term takes into account the rate of change of the error and adjusts the input based on the derivative of the error. This helps to stabilize the system and reduce overshoot.

The PID control, although best, cannot be applied in this case due to 2 separate mechanisms in action – Coarse and Fine. If the system overshoots, it cannot come back as a reversal of motion would require reengagement of the coarse drive shafts, which is time consuming. As a result, P control is chosen. Even though it is feasible relying on P control isn't the solution as the proportional constant can't be removed. Hence a custom adaptive control was employed.

Adaptive control uses a learning constant of proportion which is adjusted based on the target value for stability of system. It was observed that the system could be controlled with a precision of 100 nm with this method. Due to the limitability of the LVDT, further control could not be done. A flow chart for the control algorithm is given below. The entire control loops and all the subsequent control algorithms and mechanisms are coded in python in the raspberry Pi.

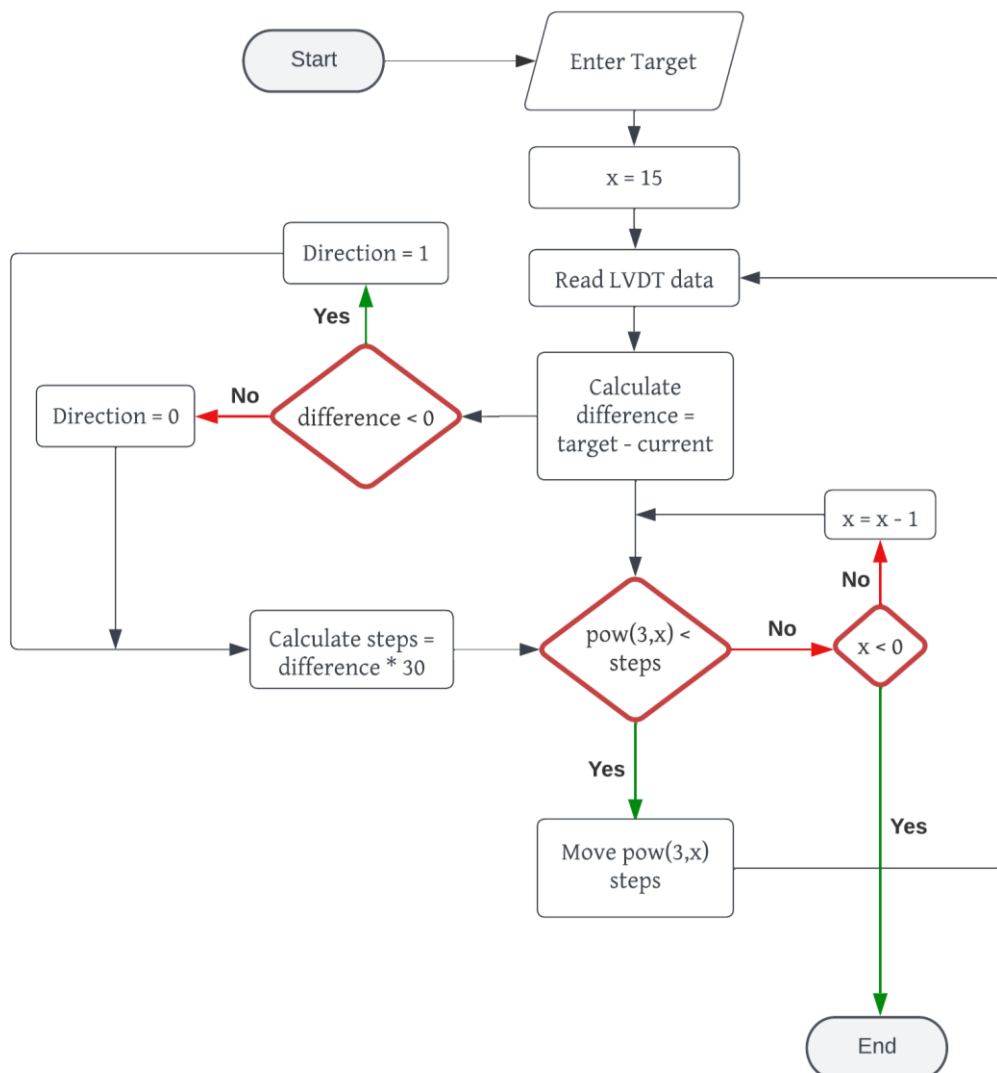


Figure 24 Coarse motion Control Algorithm

Continuous data points would enable in hunting of the target value which is most feasible method, but the LVDT does not allow continuous data acquisition. If tried, the speed of motion is drastically reduced which would take the time to position the actuator as high as half an hour. Adaptive P-control increases its rate of data acquisition as it nears the target value taking only a minute or 2 to reach the desired position. An example of controlled LVDT movement from 0 to 1000 microns is given below. It can be seen from the second graph how the current values slowly converges as it approaches the target. The cross points represent steps at which a data measurement was taken which totaled around 29700 steps of the motor.

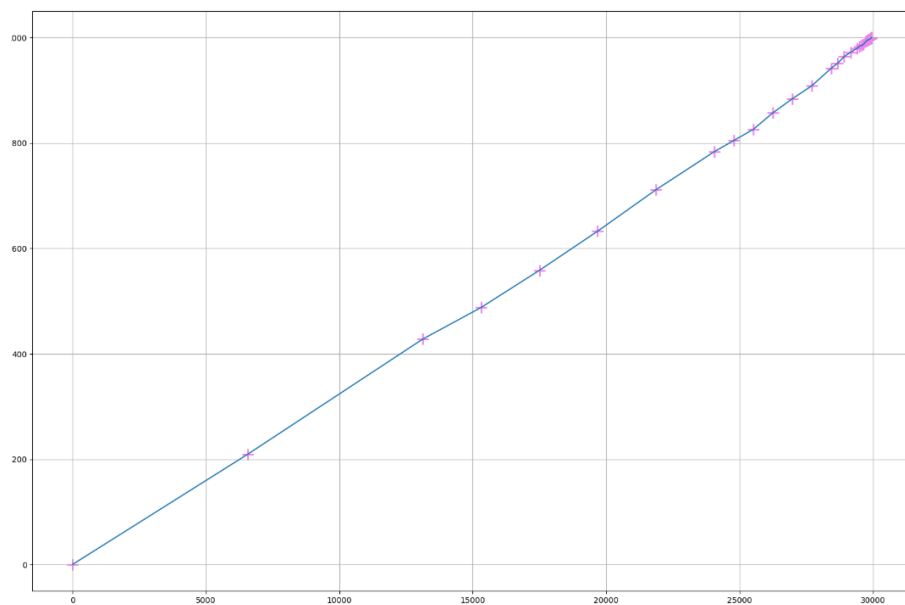


Figure 25 Linear Adaptive P-control

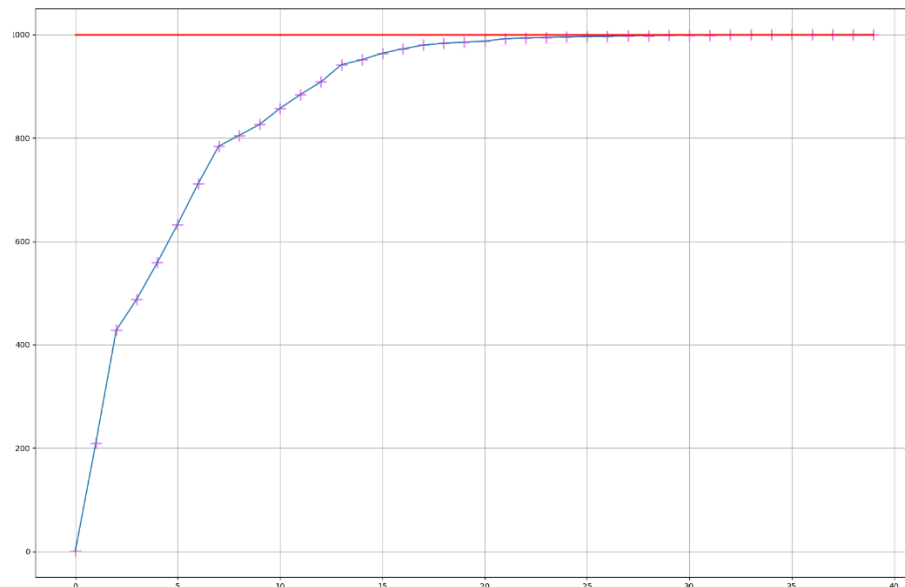


Figure 26 Convergence of Adaptive P-control

3.8. Fine Control Mechanism

The Fine motion of the actuator is governed by the ‘A’ flexure mounted with the eccentric shaft. Our results show a range of 14 microns in this actuator. Since the coarse motion can reach up to 100 nm, the rest can be compensated by the fine motion while in the backlash of the coarse drive coupler. Since the backlash provided is 300° , as a factor of safety, 270° is considered for the final operation to prevent re-engagement of the ball screw. A flow chart for the control algorithm is given below. The entire control loops and all the subsequent control algorithms and mechanisms are coded in python in the raspberry Pi.

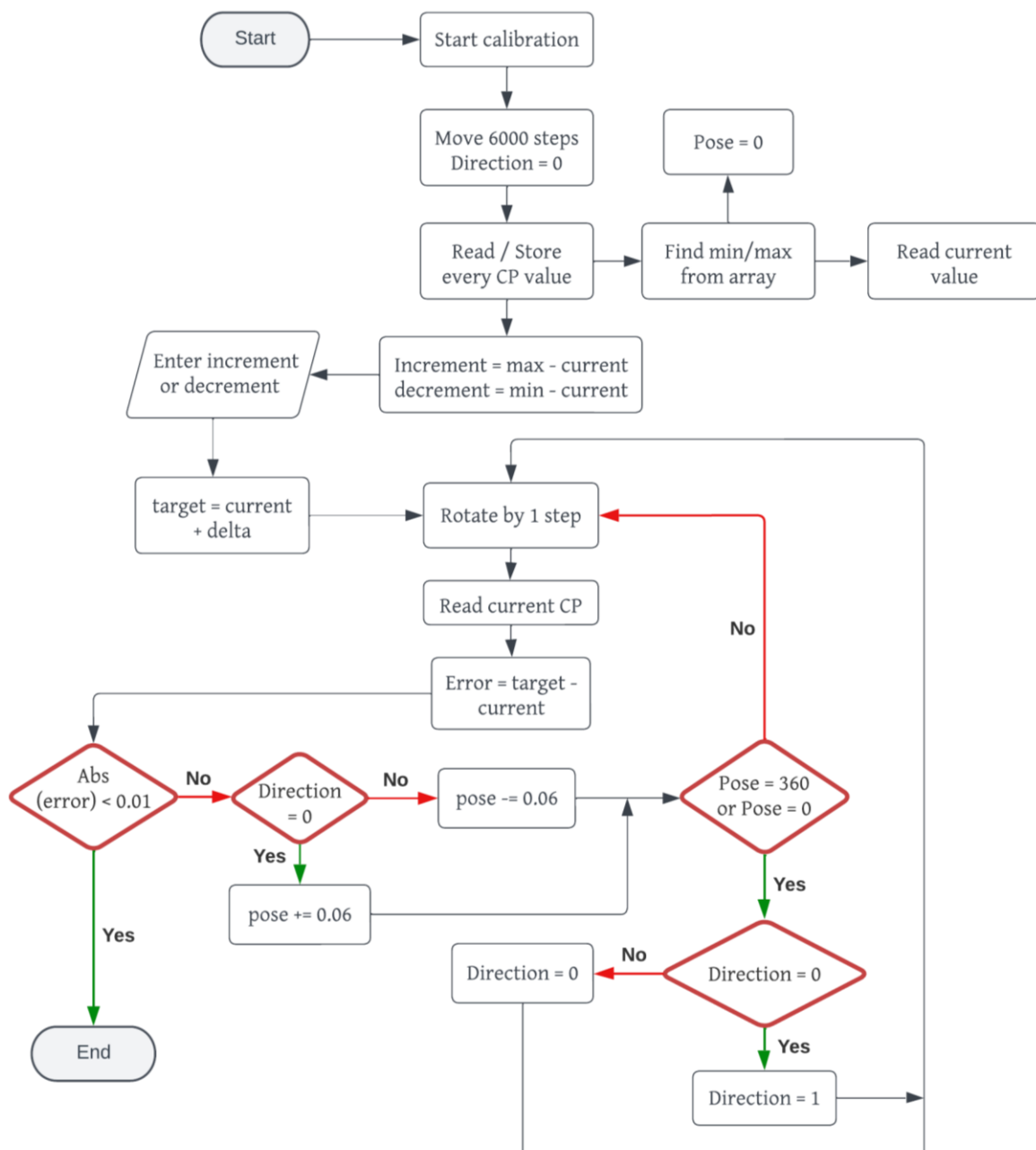


Figure 27 Fine Motion Control Algorithm

After the coarse motion ends, the current fine position of the MRS needs to be known along with the possible increments and decrements without engaging the ballscrew. A calibration before the start of every fine control is performed which retrieves current data, the maximum possible increment and the maximum possible decrement. If by chance, the required movement exceed the limits found, the coarse motion is enabled until it reaches the range of fine operation.

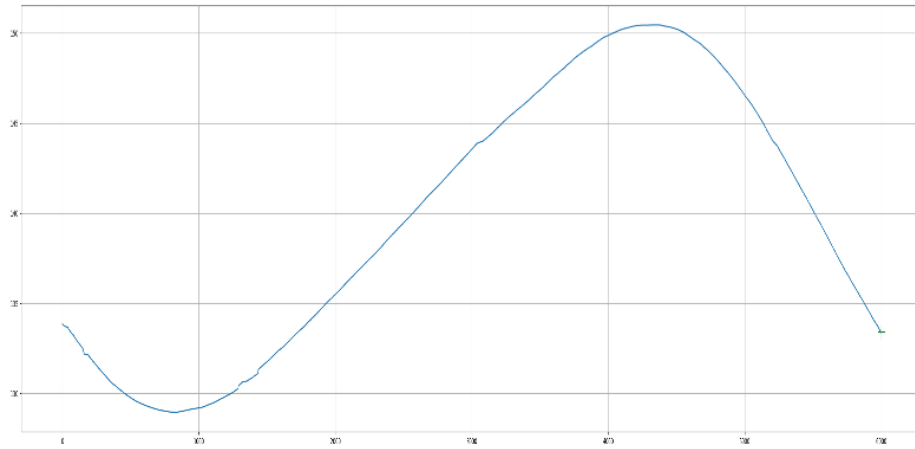


Figure 28 Calibration of Fine Motion

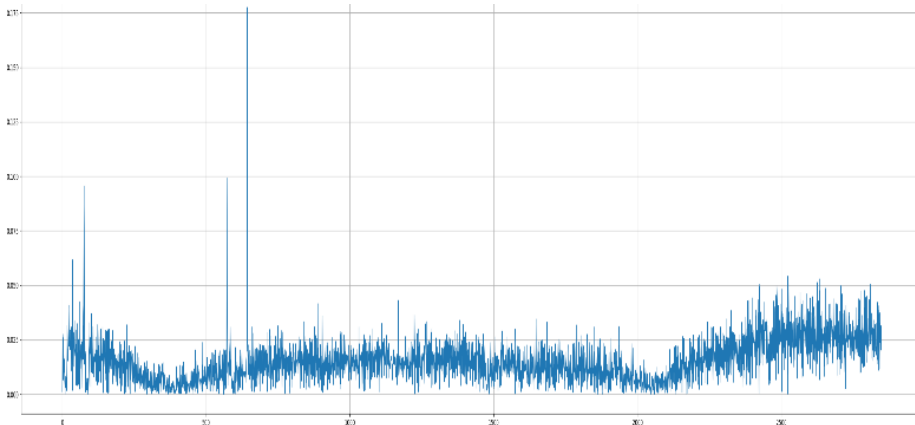


Figure 29 Step size per Revolution

One of the advantages of fine control is that data acquisition at every step is possible which enables hunting for the desired value while fine tuning. Though hunting is a plus, the nature of the MRS movement (sinusoidal) does pose a challenge as hunting isn't linearly proportional but varies along the sine wave. Thus, a control mechanism for fine tuning was developed which hunts the desired value based on rotation of the motor rather than linear distance available for tuning.

Another challenge posed by this control system is the disturbance of actuator when hunting. While calibrating and hunting, there is a tendency to change the y-values of the sine wave resulting in a shift in either axis. Thus, after every step, the values at that step are updated as well resulting in active extremities which slightly vary in resolutions of few nanometers. An example of hunting and active update is given below. From this we can also observe that at times, the actuator can miss the target value due to jumping over the target due to high step movement at that location. This is resolved by a repeatable hunting until the desired value is found.

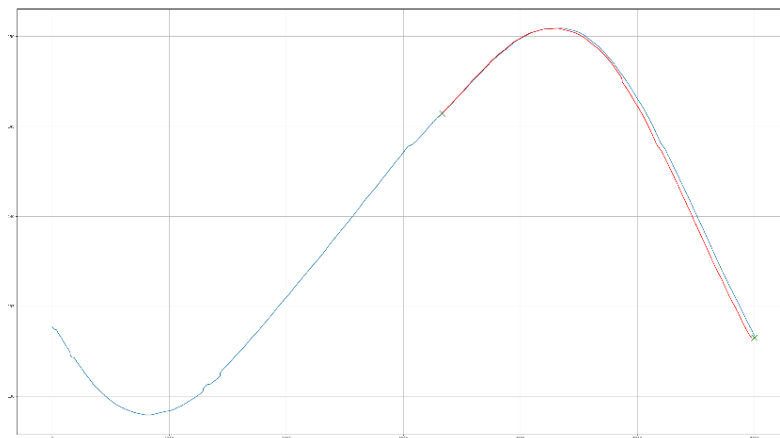


Figure 30 Hunting-1 After Disengagement

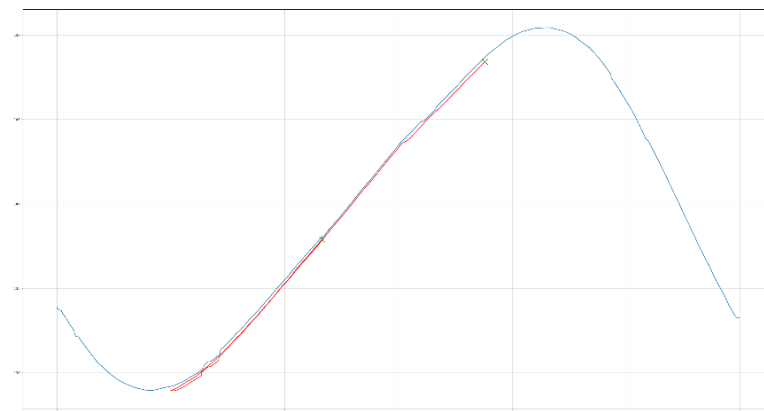


Figure 31 Hunting-2

3.9. Combined Control Mechanism

The final Actuator motion needs to be a combination of both the control mechanisms. The Fine motion gets displaced when coarse motion is enabled and when it is complete, it is highly likely that the MRS position is not the same as before. This results in an error which is smaller than the range of the MRS but still unaccounted for when operating coarse and fine together. An

algorithm using the 2 established algorithm is made which controls the combined motion. Inaccuracies such as errors while calibration of CP as well as the errors incurring in ball screw due to the fine motion is reimbursed in this algorithm. This ensures that a finite distance is travelled by the actuator down to nanometers. All the algorithms used in these mechanisms have a limiting condition of error being greater than 10 nm i.e. the motion and hunting pertains as long as the error is greater than 10 nm of the target value.

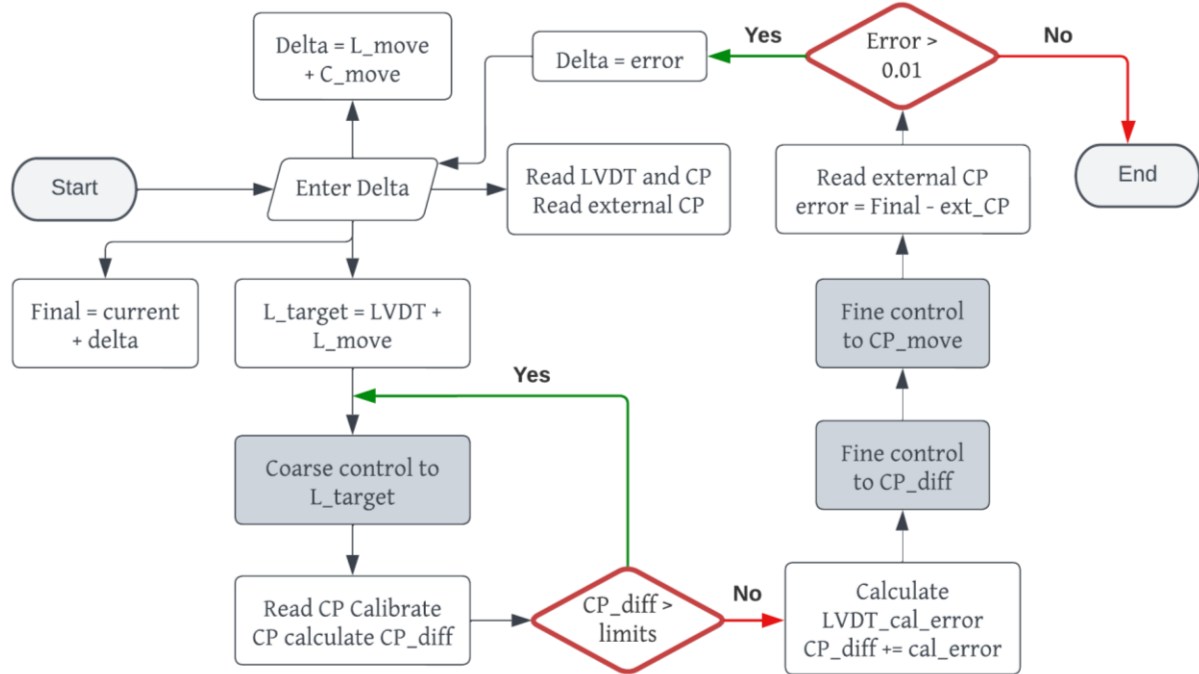


Figure 32 Combined Control Algorithm

3.9.1. Mathematical verification

The algorithm works on the principle of splitting the target positions to coarse and fine and then compensating any errors incurred during the operations. The main objective of this control system is to bring the CP movement back to its original position before coarse movement, later controlling the fine movement required which allows an access of ± 100 nm of movement from the current position allowing it to reach the target without any engagement with the ball screw. The mathematical verification is provided below.

- Current LVDT = L_1
- Current CP = C_1
- $\Delta = D_1 = L_{move} + C_{move}$
- $\Delta = LVDT \text{ movement} + CP \text{ movement} = L_{move} + C_{move}$
- Target = $L_1 + D_1 = L_1 + L_{move} + C_{move}$

- *LVDT goes to*
 - Goto = $L1 + L_move$
- *Calibrate CP*
 - New CP = $C2$
 - New LVDT = $L2$
- *LVDT error while calibrating:*
 - $LVDT_cal_error = (L1 + L_move) - L2$
 - $CP \text{ error} = C1 - C2$
 - $LVDT \text{ error} = \text{Target} - L2$
 $= \text{Target} - L2$
 $= (L1 + L_move + CP_move) - L2$
 $= CP_move + ((L1 + L_move) - L2)$
 $= CP_move + LVDT_cal_error$
 - Combined error = $CP_error + LVDT_error$
- *Goto Combined_error*

3.10. Basic GUI design for controlling Actuators

After the testing of the prototype actuator, several more actuators were needed to be assembled for the eventual hexapod system. While the parts were being fabricated, my friend and myself started working on a software which could run the actuators and the entire system without needing to open the code and run it. The software was developed using the Dash framework, which is an open-source Python framework for building web applications. The Dash framework provides a simple and intuitive way to build interactive web applications, and it allowed us to develop a web app that could be accessed using any device with a web browser. Dash provides a rich set of built-in components, such as graphs, tables, and forms, that can be used to build a web app quickly.

The software development phase of the project involved several iterations of design, coding, and testing. The design of the user interface was critical to ensure that the app was easy to use and that users could quickly and accurately control the system. We established the socket connection of the code with raspberry pi and the controller of the capacitance probe which continuously sends data to the app. It became a huge advantage as continuous stream of measurements of LVDT wasn't possible via Pi. The Pi consumes a lot of time decoding the data read from the display of the analog to digital converter, while in this case, direct

transmission of data happens saving computational time. The Pi could only perform one function at a time, but with the help of multiprocessing, this app can control as well as perform live plotting of the data. Some initial iterations and my contribution of the app is shown below.

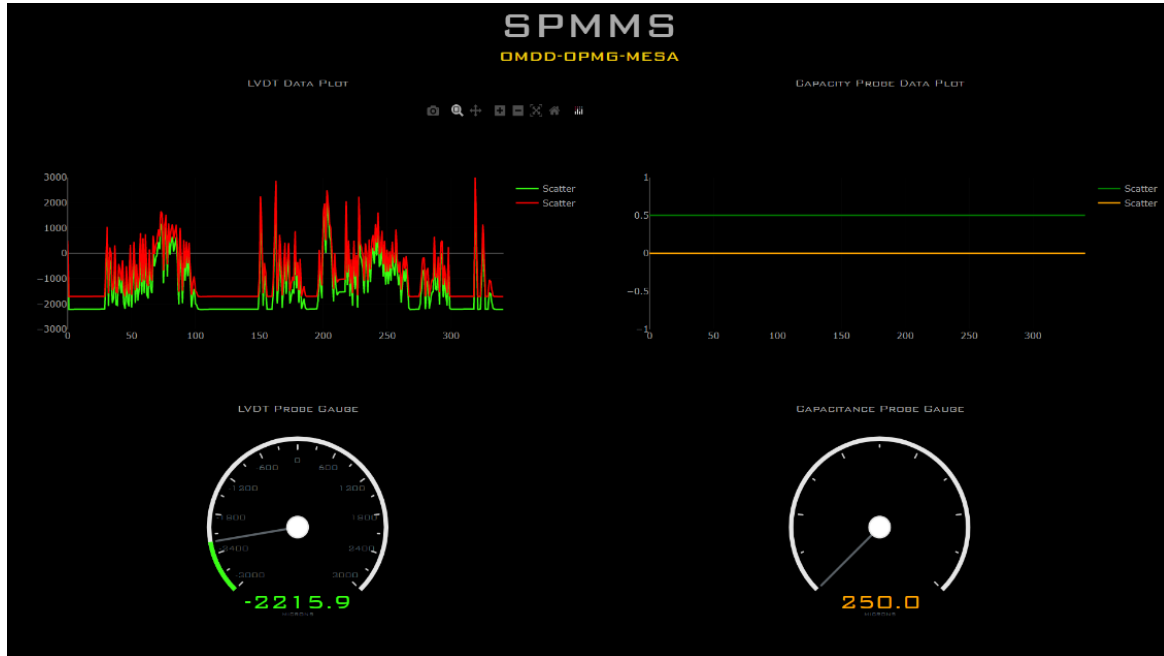


Figure 33 Initial GUI Design

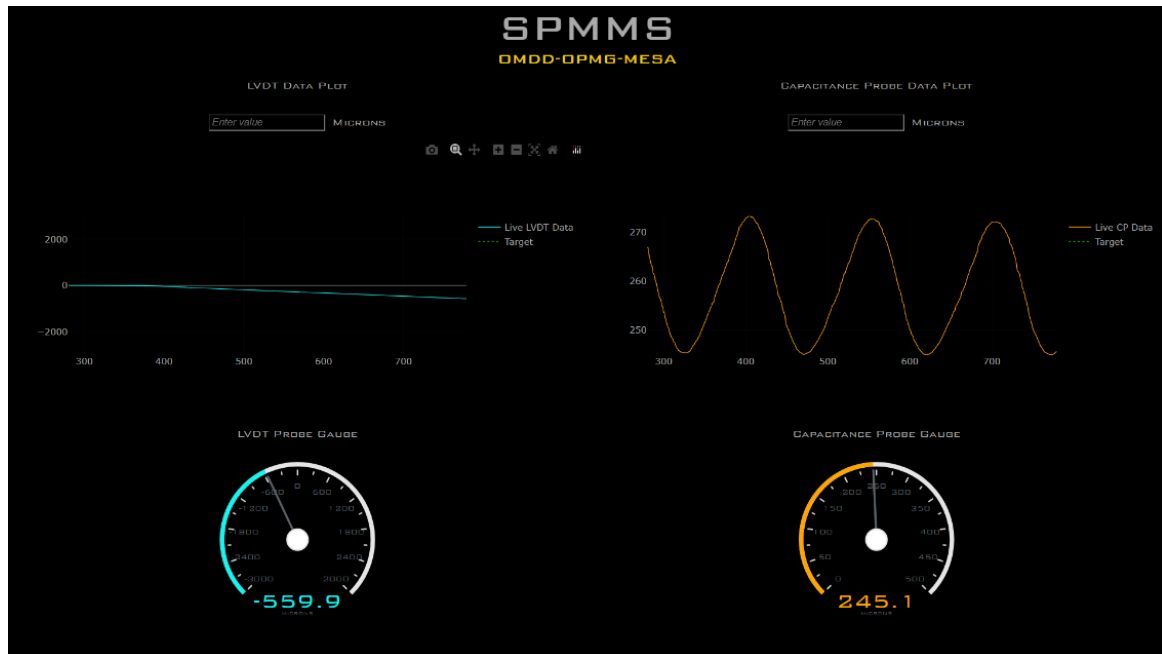


Figure 34 Dual Data Acquisition

4. Addressing discrepancies and ensuring consistency

As the combined closed loop control of the Actuator was tested repeatedly, it was soon discovered that the internal movement of the actuator after the closed loop code did not match up with the external sensor that was mounted to the table rigidly. To verify the discrepancy, the coarse drive coupling mechanism was removed and the MRS was operated alone with 2 sensors: 1 below and 1 on top of the top land of the MRS which continuously recorded the movement of the MRS. The data revealed that the internal movement is very smooth and the movement sensed externally had vibrations and fluctuations throughout the movement. Another critical problem noted included the mismatch between the MRS movements. In theory if the mechanisms are rigid and 2 measurements are taken on 2 sides of the rigid element, the resulting observed movement should be same as well. From the tests, it could be seen that the external movement produced an unknown shift in the movement at the top displacing from the movement observed internally. A graph depicting the mismatch is shown below.

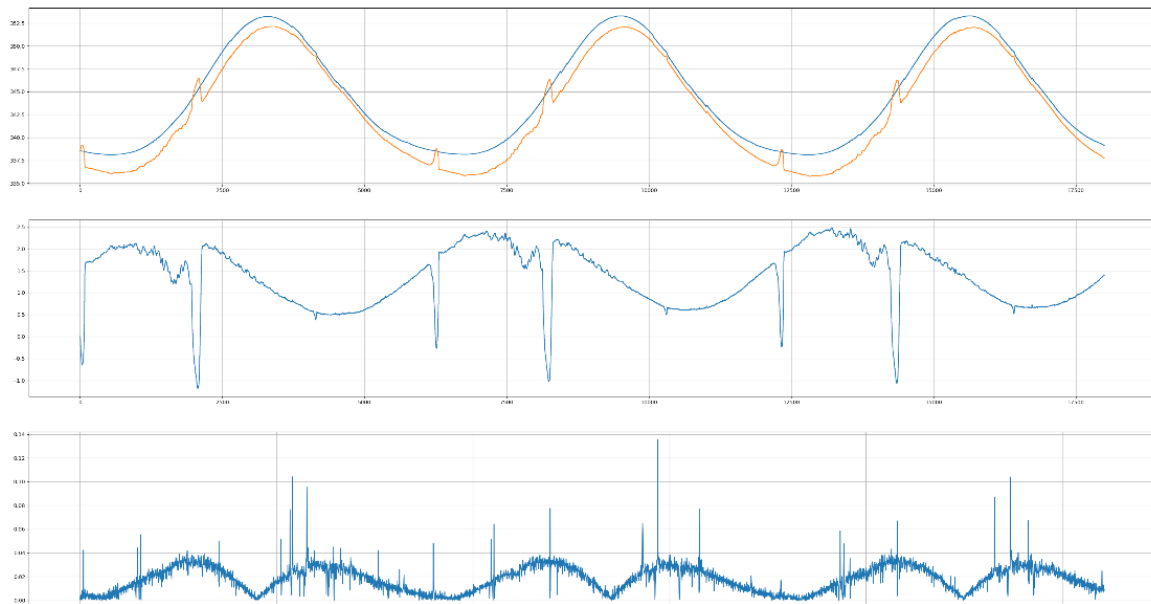


Figure 35 Mismatch observed b/w internal and external movement

The orange line shows the measurements from the sensor mounted with the table and the blue line shows the internally measured movement. The second graph shows the difference of both movement at every step. We can see the difference is significant and as high as 4 microns. The third graph evaluates the increase in variation at every step. As we can see all the graphs are sinusoidal in nature resulted from a constant shift from the internal movement.

Due to the inconsistency, there was a need to characterize the movement of the MRS with the motor steps. Accurate positioning of the MRS is very critical to this project

4.1. External Repeatability Testing

First and foremost, the verification of the repeatability needs to be done in the actuator. If a value x is read by the sensor at the motor step y , then the same value or a value under 10 nm should be read when the motor reaches that step again. For this test, we ran the motor in a full loop 10 times back and forth. Each direction was superimposed on itself and the iterative differences of each motion was measured. It was surprising to find that a ‘DNA’ like structure was plotted where each iteration was phase shifted as well as vertically offset from the previous. The following graph shows 10 such iterations back and forth.

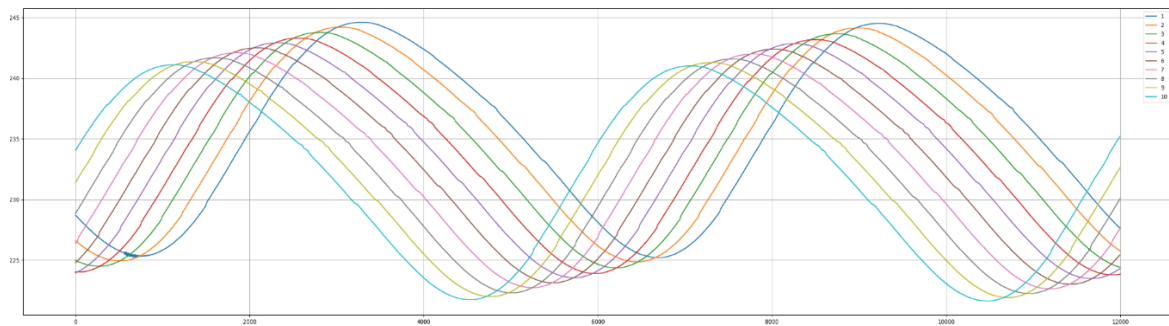


Figure 36 Initial disturbed plot

To tackle this problem, we tried different test cases including but not limited to different positions of sensor, recalibrating the motor, disassembling and assembling the critical parts of the actuator etc. Eventually as we reduced the speed of the motor down to 12 rpm from 21 rpm, the vertical shift started to wane. Eventually, at 9 rpm the vertical shift was removed up to a resolution of 1 micron at max reaching to a conclusion that the speed of motor affects the actuator assembly as a whole slowly shifting the MRS over time. The slower movement is smoother and more stable and the rough operation.

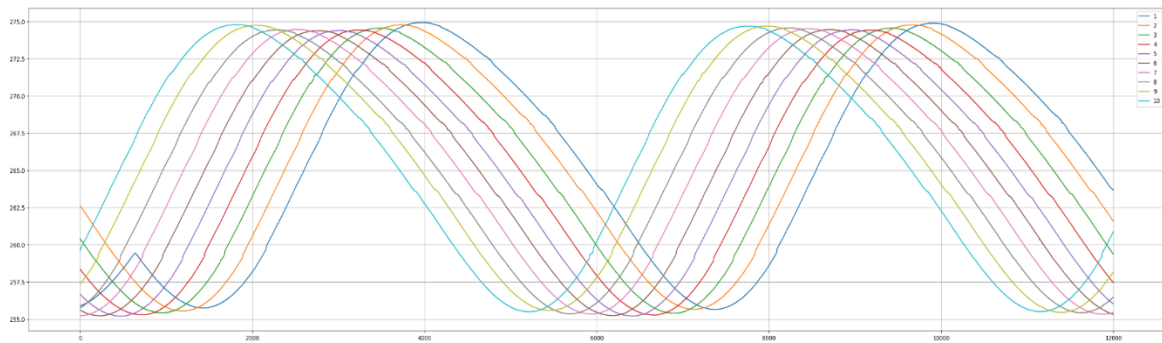


Figure 37 Vertical Offset removed

A phase shift occurs when the sine wave is shafted by an angle which means that every time the sine wave is repeated, some angular movement is lost in the movement. Since every step

moves the motor by an angle of 0.18° , we started running the same tests decreasing the motor steps required for each revolution by 1 in every experiment. Soon we found that at 1980 steps, an almost perfect overlap is produced. The iterative offsets produced from this experiment toned down to 0.8 microns. The overlapping graph is shown below.

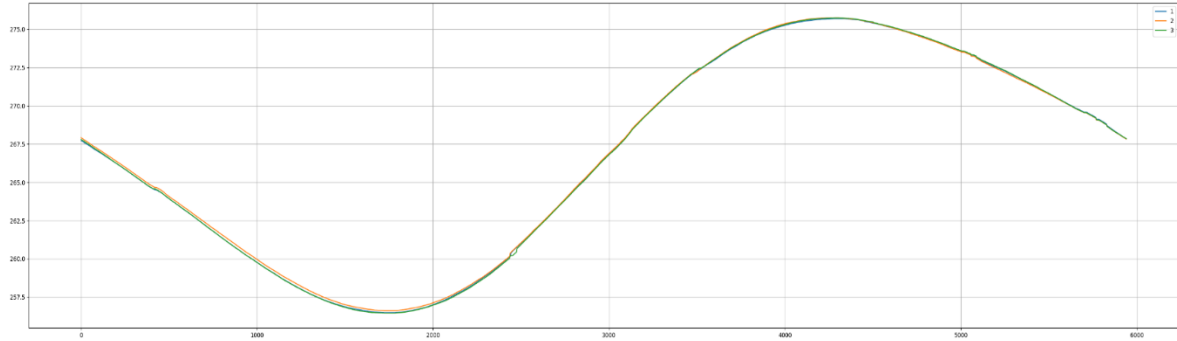


Figure 38 Phase shift removed

4.2. Mass experimentation

Having the phase and vertical shift removed under a range of 1 micron, now the repeatability was checked again with more parametric variation. The tests included further decrease of rpm to as slow as 0.3 rpm which resulted in the duration of tests capping at 3-4 hours. At the same time, we also started increasing the number of iterations to 20, 50 and 70 the experiments revealed that even though the repeatability is very high but still falls short of the required value. When the iterations reached 70, we could start seeing the vertical shift again, albeit small. Some of the many plots are shown below and a compilation of data is also provided. Soon, it was concluded that the rpm and motor steps stopped having an effect in improving the repeatability. In all the figures shown, movement in only one direction is shown. Reversed motion plots are the same as forward plots.

Tests	Iterations	RPM	Iterative offsets (nm)	Cumulative Offsets (nm)
1	10	12	160	200
2	10	15	200	563
3	10	0.3	50	120
4	6	0.9	200	200
5	50	3	290	2500
6	20	3	220	460

7	10	0.9	60	135
8	70	3	310	2700

Table 12 Summary of Mass Experimentation

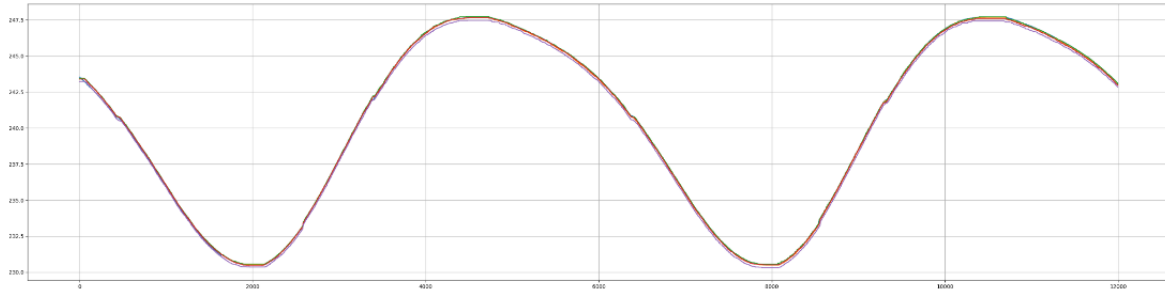


Figure 39 Repeatability under 10 iterations

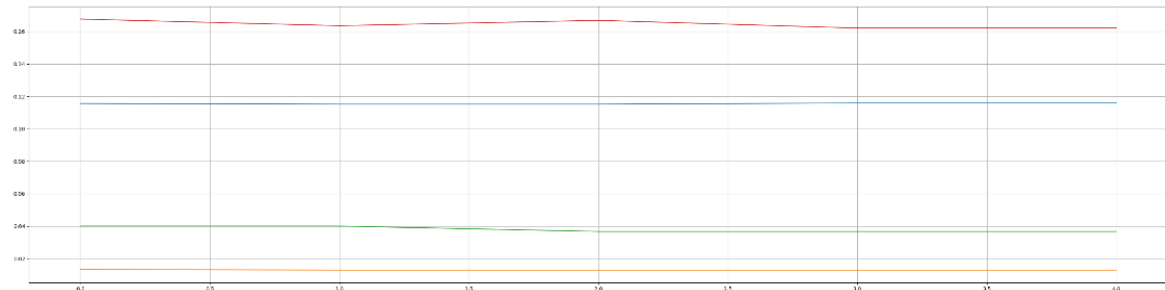


Figure 40 Offset generated by 10 iterations

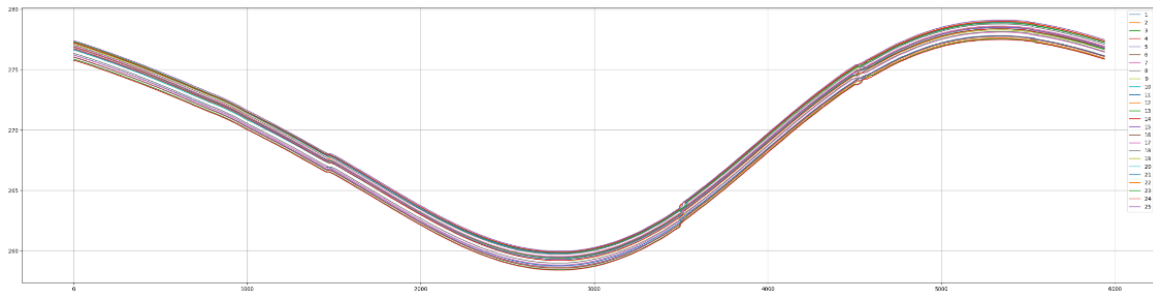


Figure 41 Repeatability under 25 iterations

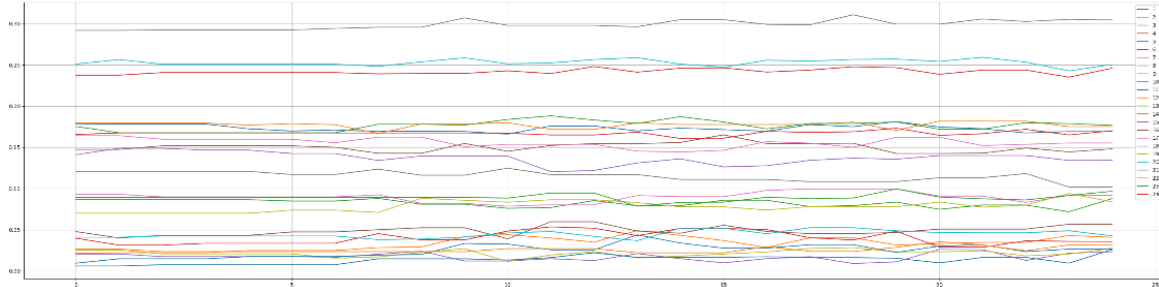


Figure 42 Offset generated by 25 iterations

From the above tests we concluded that the actuator is working properly and the errors were minimized as much as possible. The next element in this setup are the sensors. All the parameters of the actuators that could be varied were changed all to no avail. Experimentation on sensors soon began.

4.3. Stability check

If the values are changing at every iteration, one possible reason for the change could be that the sensor isn't rigidly held and is slipping constantly due to fatigue. This possibility was soon rejected as the sensor was mechanically held indirectly to the table itself. The strong latching couldn't cause slippage over time. The sensors needed to be checked over time instead. This experiment focuses on the stability of the sensing element of the CP. The sensors were kept undisturbed for 30 mins and the frequency of measurement reduced for precise measurements. The results are shown below.

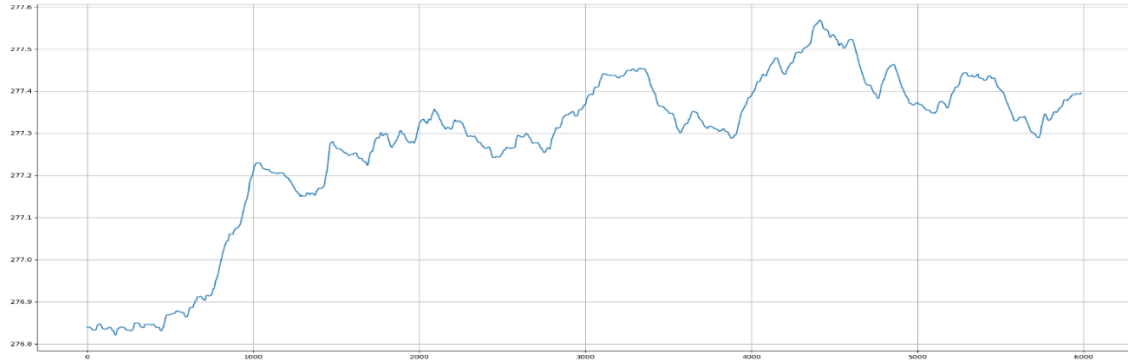


Figure 43 Static CP error

It was observed that the CP errors ranged 400, 700 and 1400 nm in 3 different sensors over 30 minutes of measuring. The test setup for the CP is made up of aluminum which has a coefficient of thermal expansion for projects such as this. Another test setup made up of invar was then utilized it has an extremely low coefficient of thermal expansion, meaning it expands and contracts very little with temperature changes. This characteristic makes it highly stable and less susceptible to thermal distortions during testing, ensuring more accurate and reliable results. Another advantage of Invar is that is dimensionally stable i.e., it maintains its shape and dimensions over a wide range of temperatures, making it ideal for applications where precise measurements and consistent performance are required. The results were satisfactory considering the change of setup.

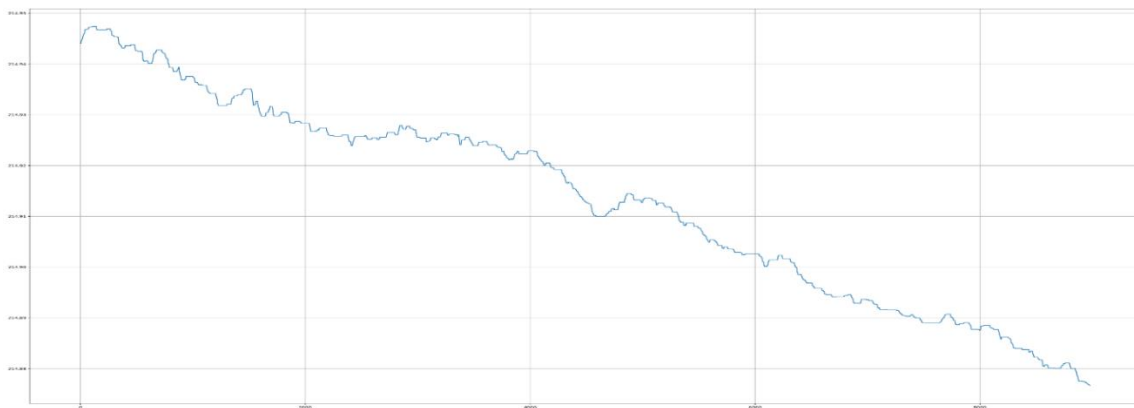


Figure 44 Static CP error: Invar

It was found that the invar setup reduced the error by 10 times giving the error values of 70, 30 and 60 nm respectively when tested over a period of 30 minutes. This study concludes that the sensor value is constantly changing over time and every motor revolution needs to compensate for this change for perfect repeatability.

4.4. Relative Repeatability.

As the values read by the capacitive probe varies over time when kept idle, it goes without saying the values changing even when the motor is moving and the revolutions are broken by the no. of steps taken. To check the validity for the invar setup, we should get the same error over time when each revolution is mapped to 0 before it begins gaining an cumulative error around 50 nm and iterative error around 5 nm based on the time and no. of iterations. After a few tests the cumulative error stayed in the same range given by the invar setup and each revolution of the motor produce an error of under 10 nm.

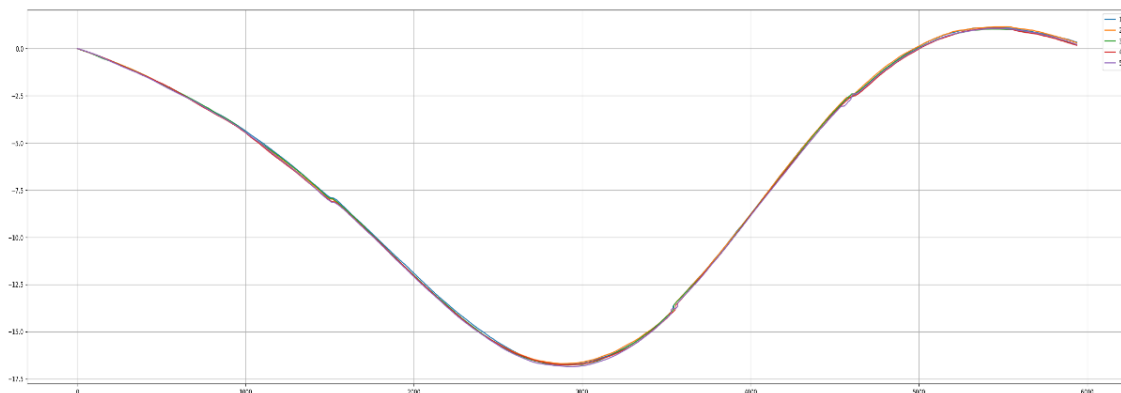


Figure 45 Repeatability mapped

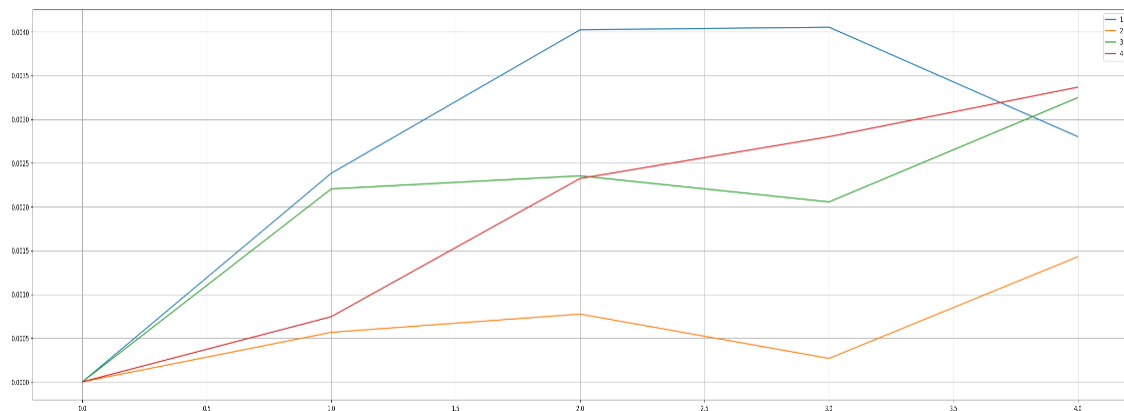


Figure 46 Offset mapped

The tests verified the fact that the sensors measurements are shifting over time and the cumulative errors cap at 60-70 nm with each iterative error being around 5-6 nms.

Due to the inconsistencies discussed in the above experiments, it can be concluded that the controlling the hexapod by noting the exact values might be difficult given we are working in the nanometer scale. A proper calibration of the sensors and a rigid mechanism assembled

professionally may bring the repeatability under 1 nm. For the time being the control action for the project will be feedback based rather than open loop using inverse kinematics. It will still be used for verification of the actuator movement.

5. Multi-Actuator Integration System and Testing

Over 20 gears of each type and several sets of all parts were delivered by the manufacturing facility at SAC. Soon after, quality check of all the parts had to be done. Pre-made parts such as bearing and ball screws had to mate properly with their mating parts to form an interference fit. While designing, the tolerances kept for critical mating parts were such that they ensured interference fit even in the worst case. For all holes, pin gauges were used to get precise dimensions. Due to the interference, axis matching of most parts becomes difficult. Careful assembly by the use of a lathe and chuck to hold the parts was done. Some of the critical mating parts are listed below, due to peculiar assemblies of these parts a correct order of assembly was also needed to be set in place. Thorough brainstorming was done to prepare a flowchart for assembly order of the new actuators as screwing fasteners and bolts would pose a problem if assembled without proper order. This stage of the project alone took 2 weeks due to the sheer number of parts and the delicacy needed for assembling sensitive parts.

- a) Eccentric shaft and bearings
- b) Bearings and actuator support structure
- c) MRS and eccentric shaft
- d) Coarse drive shafts and bearings
- e) Coarse drive shafts with bearings and its housing
- f) Ballscrew and bearings
- g) Ballscrew with bearings and Actuator support structure
- h) MRS with eccentric shaft and ballscrew with actuator structure

5.1. Integrated Drive Electronics

6 actuators will be used to create a hexapod supporting the mirror segment of the mirror. 1 raspberry Pi will be employed per mirror and 1 driver for controlling the final mirror segment. For testing purposes and easier control, 6 different drivers are connected to a single Pi for 6 motors. The USB interfaces for the LVDT and Ethernet cable for 6 CPs are also connected to Pi, acting as a single unit central controller system. The Pi is powered using 5V power supply,

while the motor drivers are powered using 12V power supply. A block diagram depicting the connections is given below.

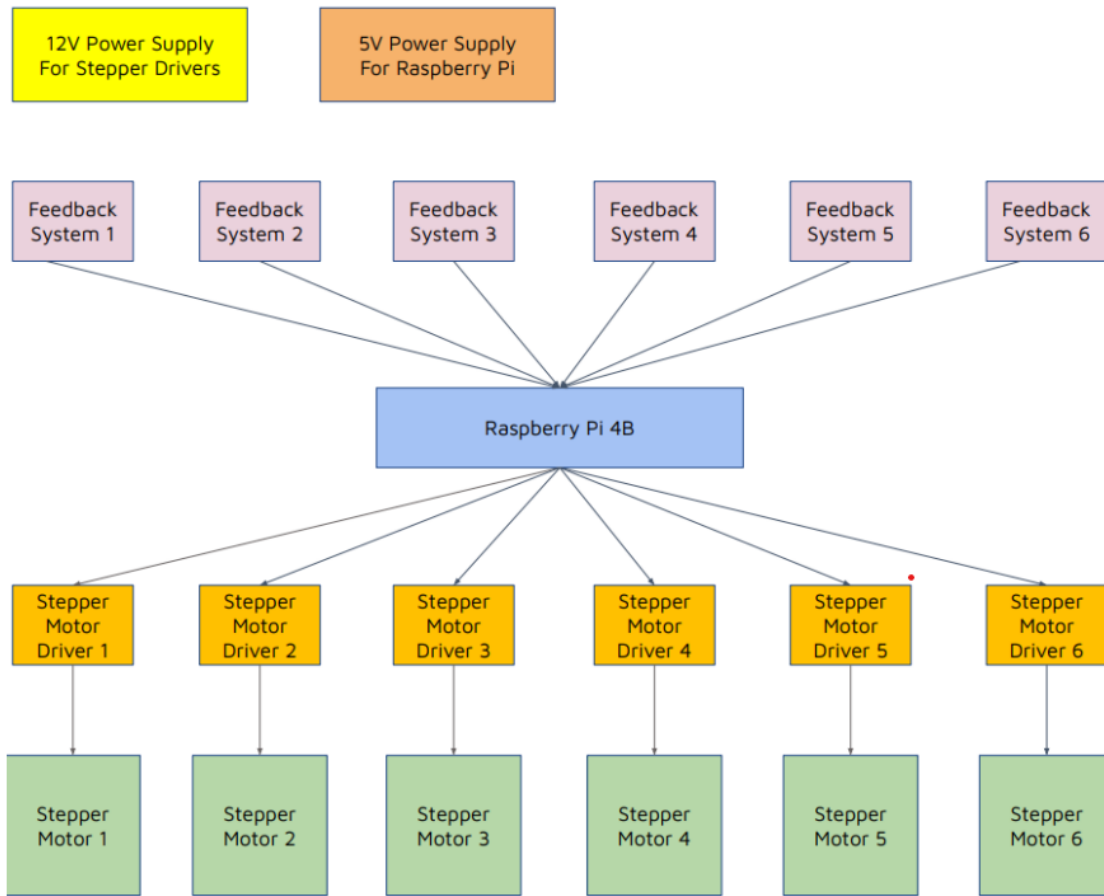


Figure 47 Block Diagram for Central Controller Unit

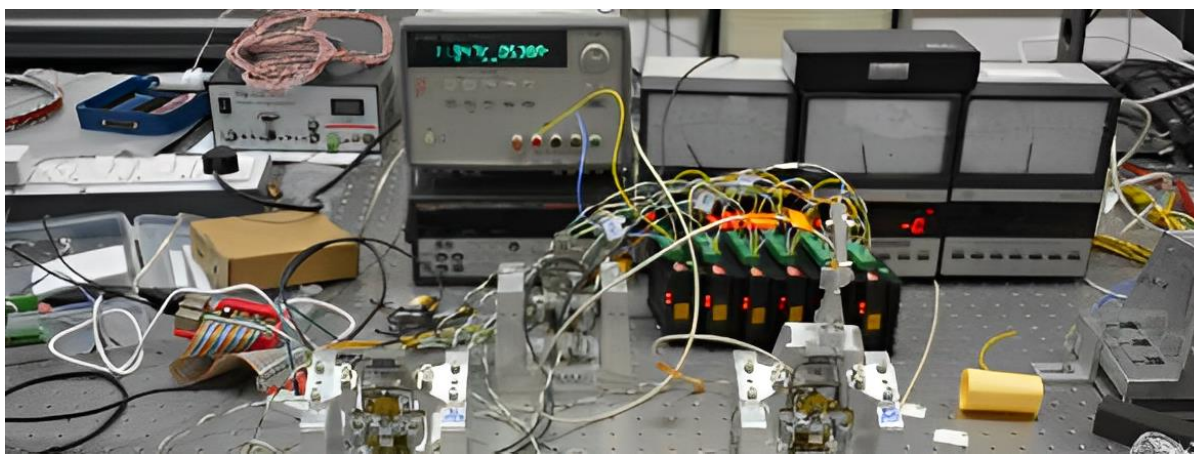


Figure 48 Drive Electronics Setup

5.2. Testing of 6 Assembled Actuators

After the assembly of 6 actuators, the range and resolution of each of them needs to be tested. There could be machining or fabrication errors in the MRS which could lead to a drastic change in their properties. The step size of each actuator was measured and a rough estimate was made about its motion capabilities based on the number of steps under 10 nm. The higher the range, less the number of steps smaller than 10 nm. The table below provides a summary of all these properties.

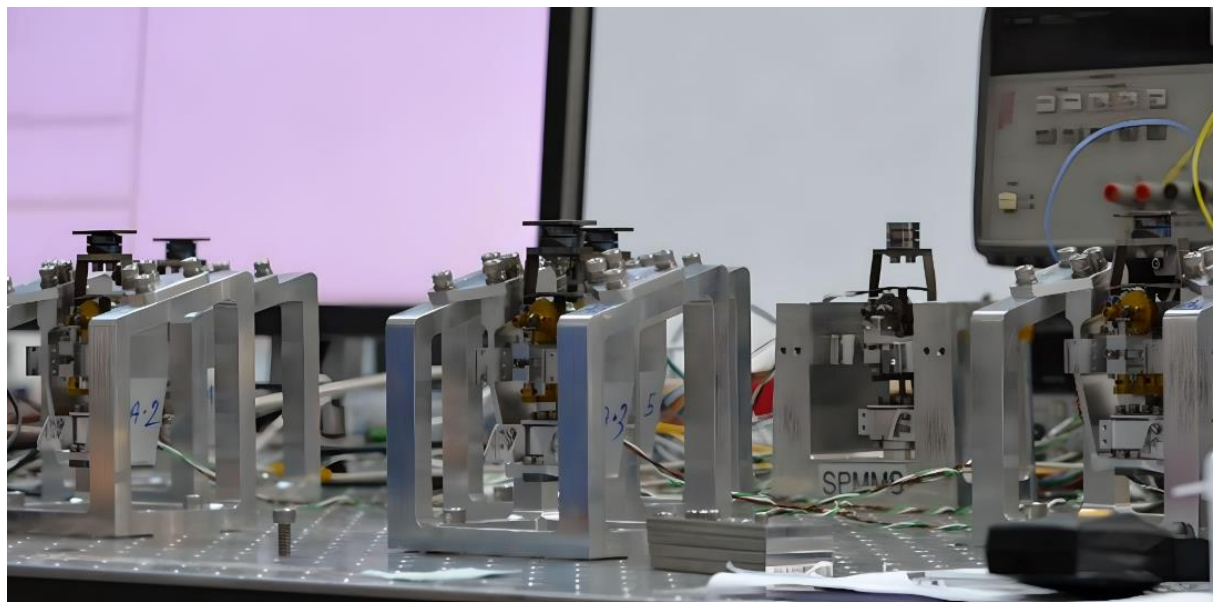


Figure 49 Testing of 6 Actuators

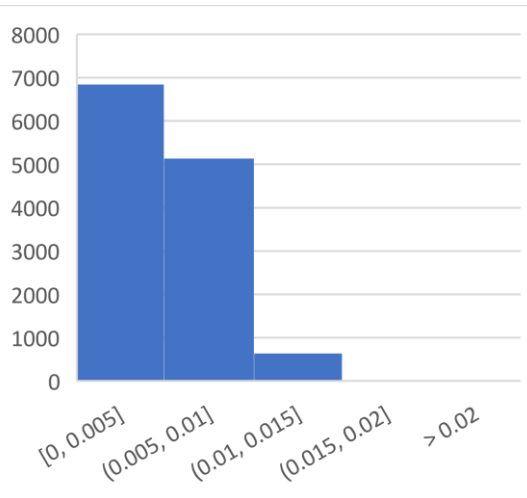


Figure 50 Actuator 1

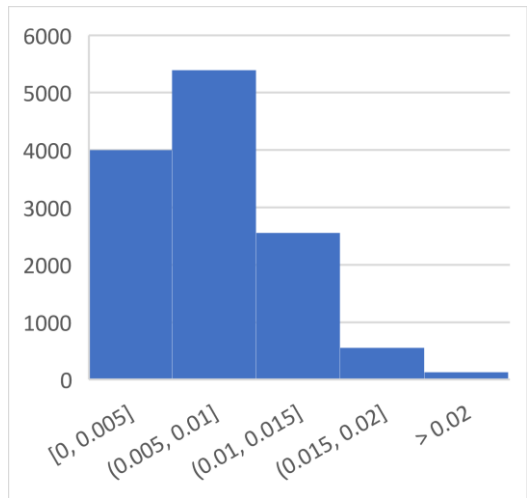


Figure 51 Actuator 2

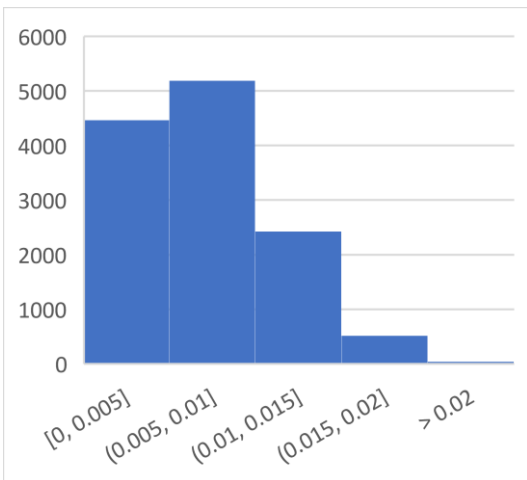


Figure 52 Actuator 3

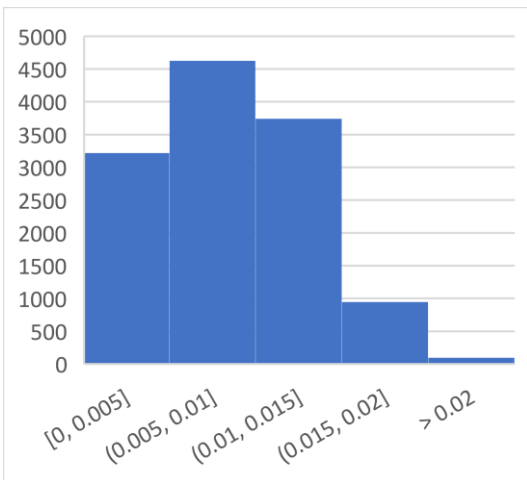


Figure 53 Actuator 4

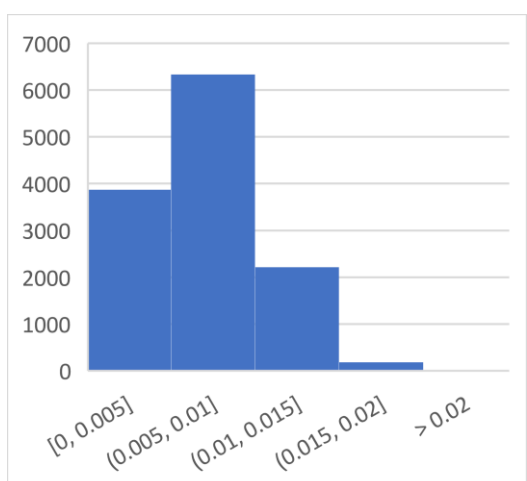


Figure 54 Actuator 5

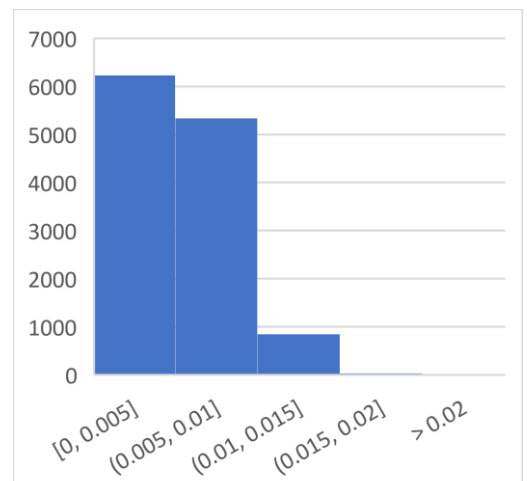


Figure 55 Actuator 6

Table 13 Step sizes of 6 Actuators

Property	Range (microns)	Resolution (nm)	Step size (nanometer)				
			0 - 5	5 - 10	10 – 15	15 – 20	> 20
Actuator 1	14.783	4.927	6841	5136	639	19 (>15)	-
Actuator 2	22.675	7.558	4002	5394	2558	553	131
Actuator 3	21.471	7.157	4467	5186	2426	516	41
Actuator 4	26.416	8.805	3221	4627	3743	948	98
Actuator 5	21.932	7.310	3873	6337	2217	187	16
Actuator 6	16.096	5.365	6232	5338	848	31	15

Table 14 Comparison of 6 actuators

From the above table, we can conclude that not all actuators or MRS manufactured can have the same range and resolution as the governing parameters for the MRS are quite difficult to fabricate precisely. Although there are some deviations, the actuators are still within our calculated error and most of them have steps under 10 nm except for actuator 4 having a range of 26 microns. From the table we can make pairs for the bipod assembly such that both the actuators in the pair have similar range and resolution. The pairs made from the dataset are:

- a) A1 and A6
- b) A3 and A5
- c) A2 and A4

5.3. Load Handling of 6 Actuators

Even though disk brake will be attached to each of the actuators, the verification of load handling capacity of all actuators along with slippage during no load conditions. From the tests some actuators caused slip when exceeded 500 grams of load while others had a solid assembly requiring no load at that weight (may slip with additional weight). With the addition of disk brake the disengagement error was verified and all the actuators showed a bearable error within 7 microns.

Actuators	A1	A2	A3	A4	A5	A6
Slippage	Yes	No	Minor	Yes	No	Minor

Table 15 Slippage of 6 Actuators

6. Bipod Integration and testing

A bipod assembly refers to a specific configuration where two legs, typically positioned on opposite sides of the hexapod, act as a pair or "bipod." This assembly allows for stability and controlled movement by providing a stable base of support. In a bipod assembly, the two legs work together to provide stability and balance during locomotion or when the hexapod is stationary. This configuration is often used to enhance the hexapod's ability to handle uneven terrain or maintain balance on inclined surfaces. By utilizing a bipod assembly, the hexapod can distribute its weight effectively and adjust its leg positioning to adapt to the environment.

The bipod assembly has the actuators inclined at an angle of 15 degrees in our case. A pad was designed which connected the top flexures of the individual actuators. The top flexures are made to substitute the free rotational movement in a macro hexapod assembly. These top flexures along with the pad provides enough rotational freedom for the actuator to move in 6 DOF without high induced stresses due to bending of the flexures and pad. A single bipod has the capability of 2 degrees of motion: z axis and rotation about the connecting plane say xy-plane. With 3 more bipod assemblies, a Hexapod can move in 6 DOF.

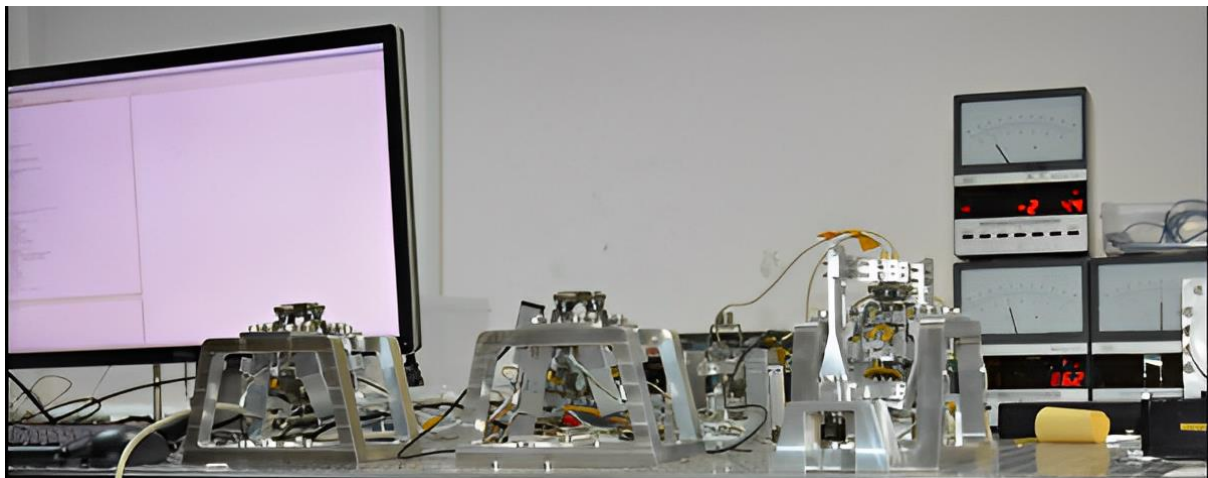


Figure 56 Bipod Assemblies and testing

6.1. Z-axis Motion Control Demonstration

The bipod in itself can operate in 2 degrees of motion. We need control the motion in these 2 degrees of motion. In theory, when 2 actuators are given motion command parallelly, they should move in z-axis together giving a constant motion. But our system incorporates 2 types of motion – Fine and Coarse, where the fine motion is the preceding motion resulting in different motions at the MRS and different positions in the backlash. Eventually they both engage and start macro movement but the resultant offset in the 2 MRS will always produce a

repeating motion when put to test. An experiment to verify this was conducted, where the actuators started disengaged randomly and then engaged to produce the macro movement. 2 CP were placed on the top of pads superimposing above the top flexures of the actuators which receive the movement of Bipod's 2 ends. In the experiment 2 graphs were plotted: the first graphs depict the movement of the actuators based on the CP and another which shows the difference of movements at each step of both the actuators.

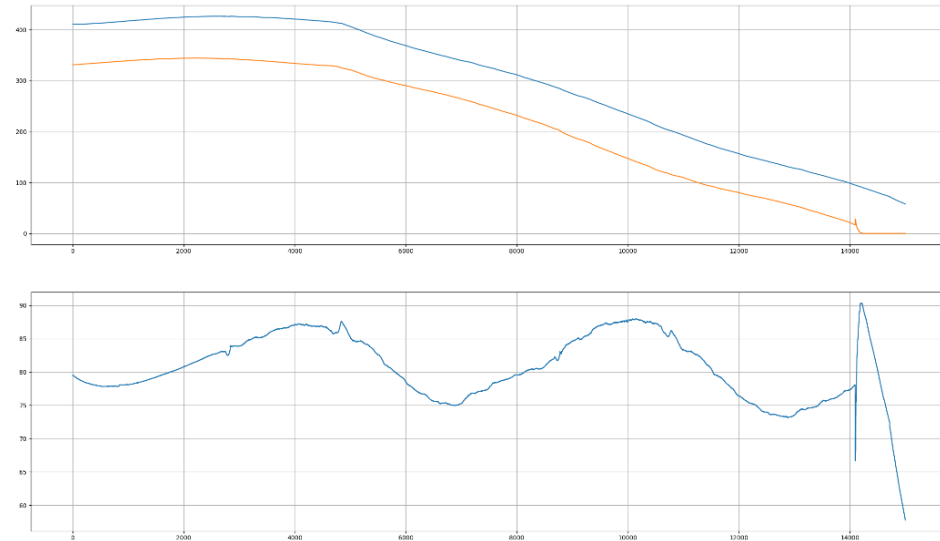


Figure 57 Bipod z-motion (Disengaged)

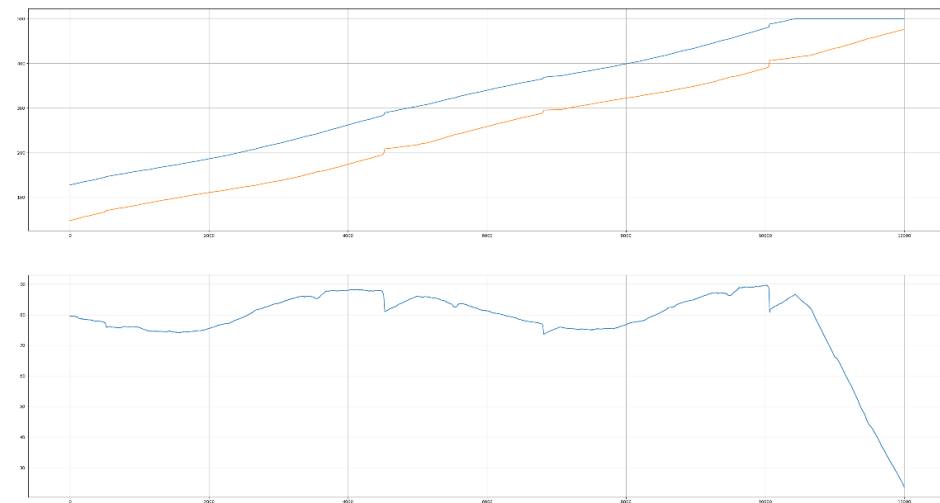


Figure 58 Bipod z-motion (Engaged)

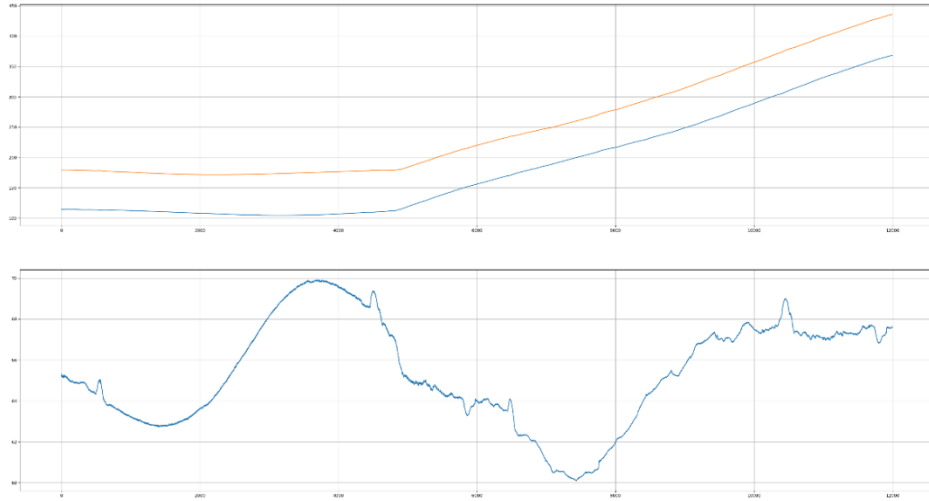


Figure 59 Bipod Motion Disturbance

The differential movement will always be a sine wave which can be mathematically verified below. It can be seen from the 3rd graph that the motion is smooth when operated in the disengaged motion and it gets disrupted during engagement. One reason for that is due to the stresses generated at the top of the pad. If the lengths are increasing then a compressive force acts on the pad creating a distorted sine wave. The same goes for when the lengths are decreasing creating a tensile force. The distortions pose a threat to our book keeping. For the prototype, feedback control is employed so the control mechanism will take care of it. In the final model, more rigid and highly will be used enabling an open loop control system.

6.1.1. Sinusoidal verification

Let's consider two sine functions $f_1(t)$ and $f_2(t)$ with the same amplitude and frequency but with a phase difference of ' δ '. Let the difference of the functions be denoted by $g(t)$.

$$f_1(t) = A \sin(\omega t) \quad (1)$$

$$f_2(t) = A \sin(\omega t + \delta) \quad (2)$$

$$g(t) = f_1(t) - f_2(t) = A \sin(\omega t) - A \sin(\omega t + \delta) \quad (3)$$

$$g(t) = 2 \times A \times \sin(\delta/2) \times \cos(\omega t + \delta/2) \quad (4)$$

- Amplitude: The amplitude of the resulting function $g(t)$ is given by $2 * A * \sin(\delta/2)$. This is a constant value, as δ is a fixed angle.
- Frequency: The frequency of the resulting function $g(t)$ remains the same as the original sine functions, which is ω .
- Phase Shift: The phase shift of the resulting function $g(t)$ is determined by $\omega t + \delta$.

Thus, we can conclude that the difference between two sine functions, when offset by an angle δ , generates a sine wave with a constant amplitude, the same frequency as the original sine functions, and a phase shift. Therefore, mathematically, the difference of two sine functions offsetted from each other by an angle δ does generate a sine wave.

6.2. Correlation of Legs of the Bipod

The top of the bipod is connected with the legs of the Bipod. It could be seen from the previous experiment that when one of the leg moves, another is also affected. This property of the Bipod is necessary to be characterized for putting the bipod in a controlled loop. Properly utilizing the reduction ratio of the movement of other actuator can reduce electrical power and time, if used effectively. The following tests showed a maximum reduction of 0.4. Higher deviation from each leg results in higher stresses leading in disruption in the rigid position. Based on the results of these experiments control algorithms to control a Bipod assembly were developed.

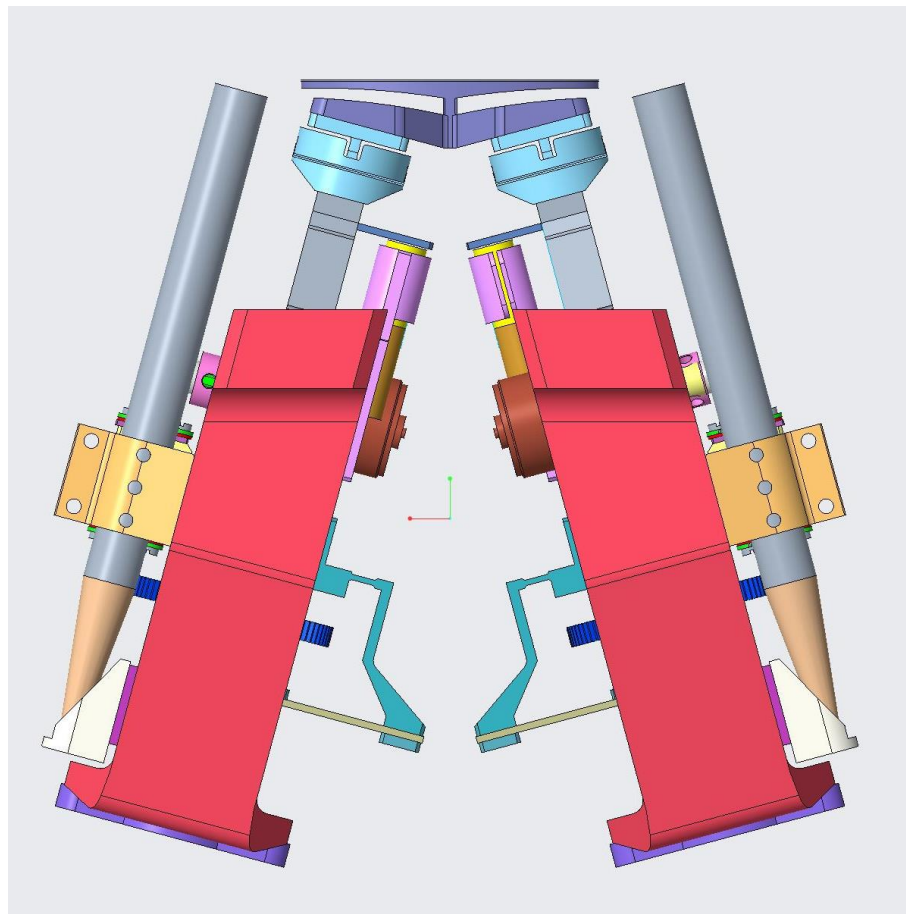


Figure 60 Bipod CAD model

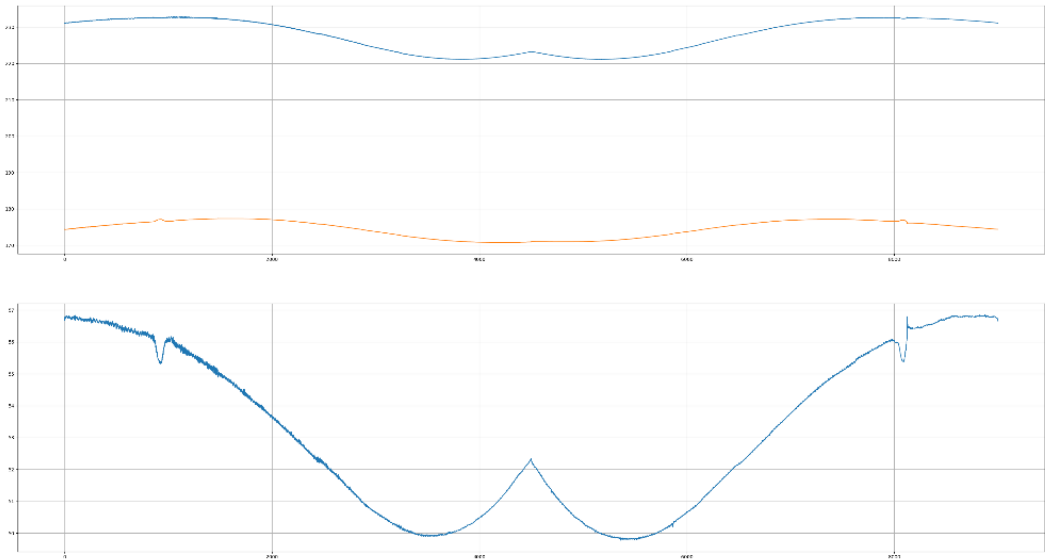


Figure 61 A2 moves A1 is Observed

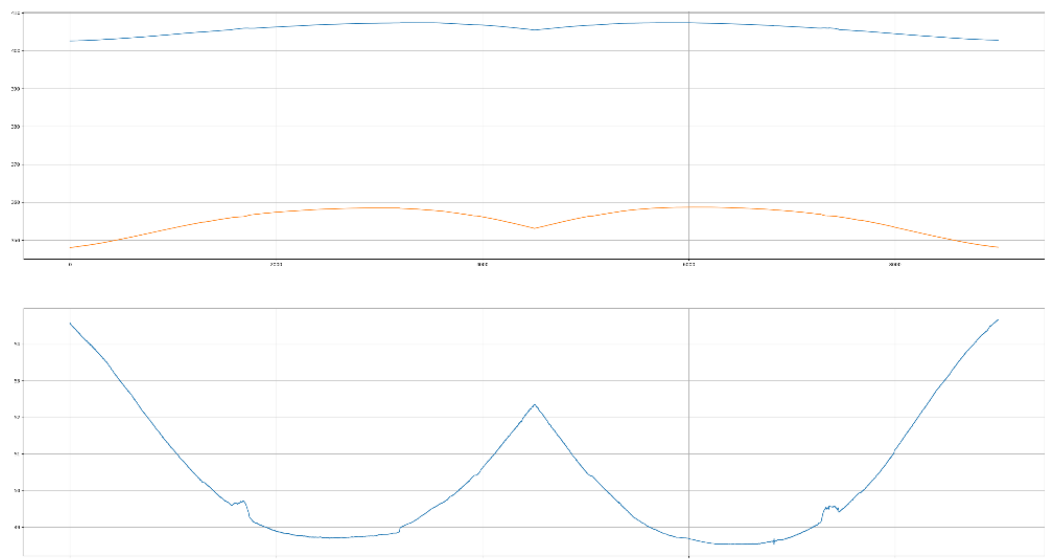


Figure 62 A1 moves, A2 is Observed

From the continuous reversal of direction of motor of the actuator to keep the motion constrained to MRS, we can see that the difference of their movement results in a sinusoidal wave. As the MRS of both the actuators reach the peak of their motion, the reduction also reduces and maximizes when the MRS is at the middle of the movement. From this, it can be concluded that the sine wave for reduction ratio/difference is phase shifted by a perfect 90 degrees. From the graph we can see the reduction ratio stays in a range of 0.35 to 0.4.

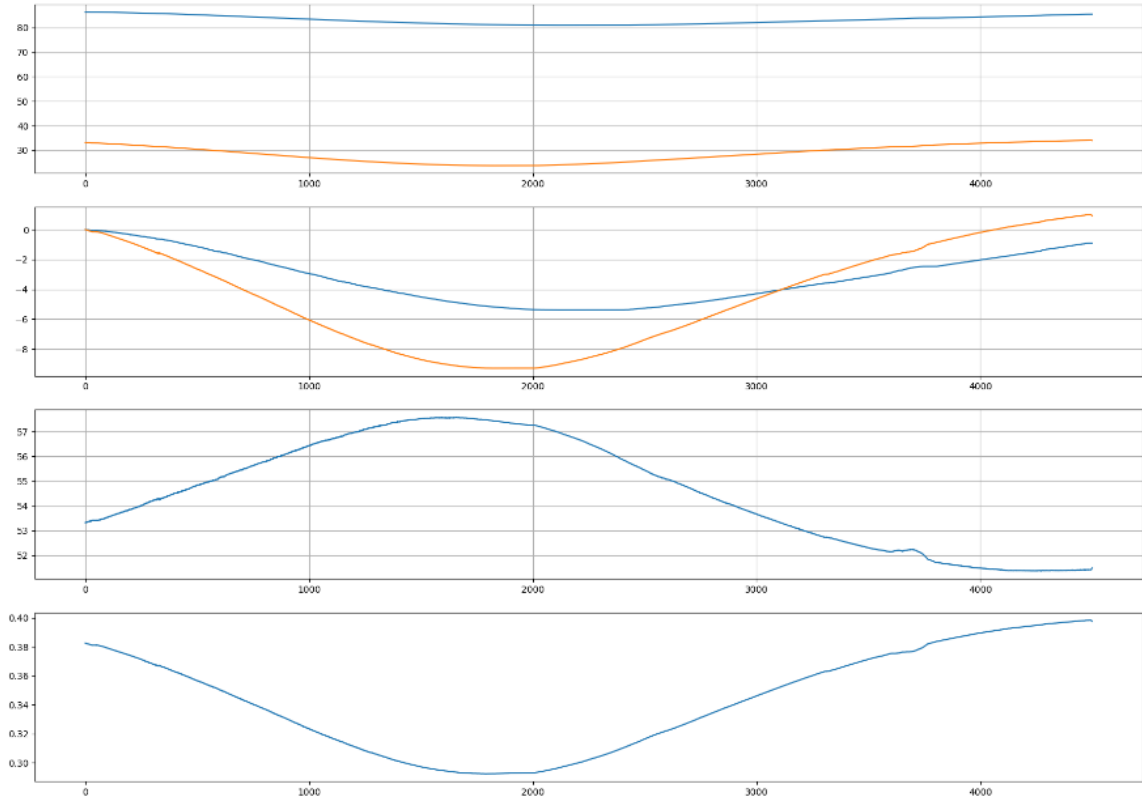


Figure 63 Correlation for Reduction Ratio

6.3. Control Mechanism for Bipod Assembly

To control the bipod in 2 degrees of freedom, both the actuators need to cooperate with each other reach the target position. As the legs are assembled at an angle of 15° , the movement of the actuator in vertical direction is reduced by a factor of $(\cos 15)$. The calculations need to be adjusted for this difference of movement. The factor of 0.9659 doesn't cause much change when fine tuning but poses a problem in inverse kinematics in coarse motion. Since the prototype is based on continuous feedback of CP, 2 capacitance probes are place on the ends of the Bipod pad. These sensors act as 2 fixed points in a line giving the slope and z-movement of the line segment. The user enters an angle to move and a z displacement. The program calculates the final position of the pad based on the input and current position and gives motion to the stepper motors. 2 control algorithms are discussed below based on stresses and time complexity of the process.

6.3.1. Independent Location Hunting

This Method works on the principle of hunting the closest point w.r.t. the final location of the bipod. The coarse motion for the first actuator begins and it hunts the target position until it gets under a range of 100 nm. The error values for both the points are checked again and the second Actuator starts moving. After the second Actuator has reached the target position, from the previous experiments, we can figure out the displacement of the first actuator due to the movement of the second and calculate the corrective distance for the actuator to move in order to align the pad again. As the first actuator is corrected, the second gets displaced and the corrective measure is applied for the second one. As the process is repeated again and again, each iteration of corrective action requires less distance than the previous to correct itself. Eventually, the bipod pad converges itself under 100 nm of range.

After the coarse motion is completed, the fine tuning begins. The corrective action of the fine motion also works in the same way as the coarse correction, correcting itself while the other one hunts the position. The different here comes from the fact that the fine motion doesn't hunt through the entire backlash. Since we know the range of error is under 100 nm, the motor reciprocates 20 steps in each direction trying to find the final position. Once it does, it moves on to the second actuator and then corrects the first repeating the cycle.

A singularity may occur in this algorithm which fails to find the necessary position in the 20-step range due to, say vibrations or noise which may disturb the actuator. In such cases a limiting timer is placed which is greater than 2 cycles of hunting providing enough time to locate it. If it can't fine the position fine tuning terminates and errors are rechecked, if the errors are greater than 100 nm then back to coarse control, otherwise keep on hunting. This removes the singularity ensuring a converging algorithm every time.

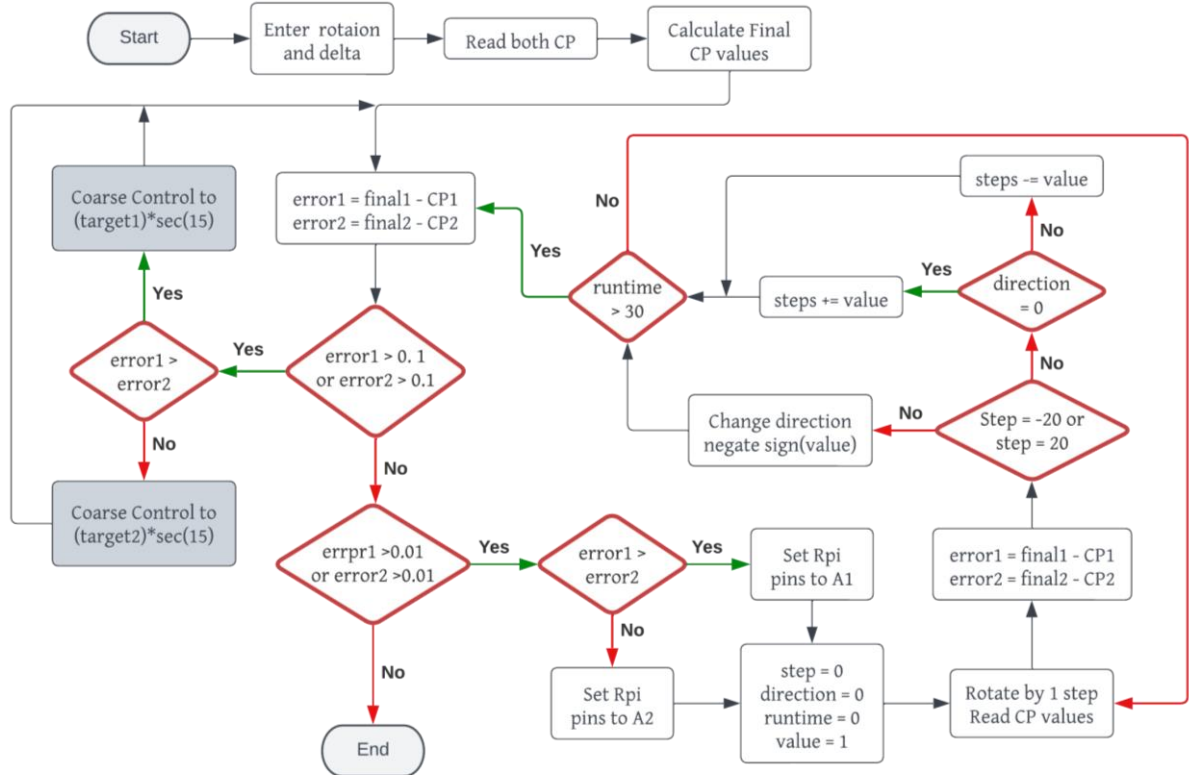
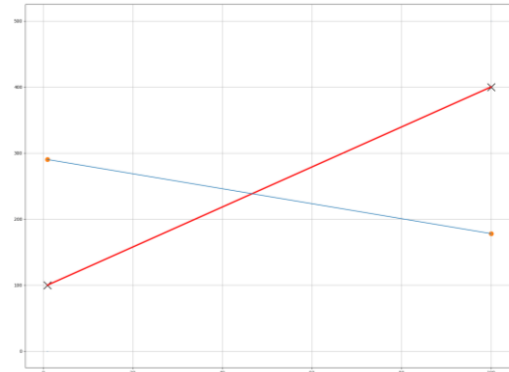


Figure 64 Bipod Independent Hunting Algorithm

Some videos and gifs of this method are bundled with this report and inserted in the ppt during presentation. The blue lines represent the current position of the actuators while the red line represents the target. All types of cases were tested and the time required to converge in each of them were evaluated. The gifs are given below which can be played in the word format.



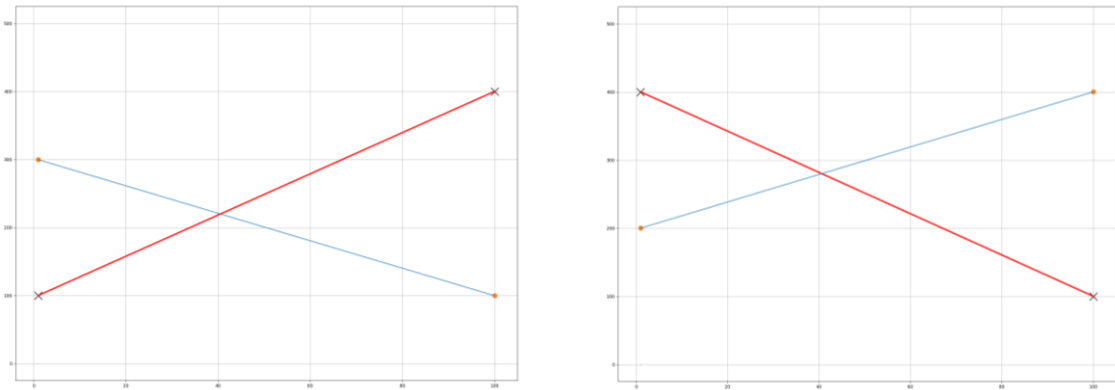


Figure 65 Test cases for Algorithm 1

Drawbacks –

- We can see that this method takes a lot of time along with high feedback count which the project aims to be as small as possible.
- Another downside of this method is the stresses that are generated when pushing one of the actuators while keeping the other stationary. If the actuators are moved to opposite extremities, the stresses induced, border the limits.
- To overcome the drawbacks, another algorithm was developed which turned out to be more efficient.

6.3.2. Dependent Location Hunting

This method proposes a dual error checking rather than pursuing target of only one actuator. The Algorithm will try to orient and displace z at the same time preventing high generation of stresses. It uses the fact that the second actuator is displaced when the first moves and uses that displacement as a form of correction. This allows the number of iterations to reduce by 4 times. And time complexity is reduced by 3 times.

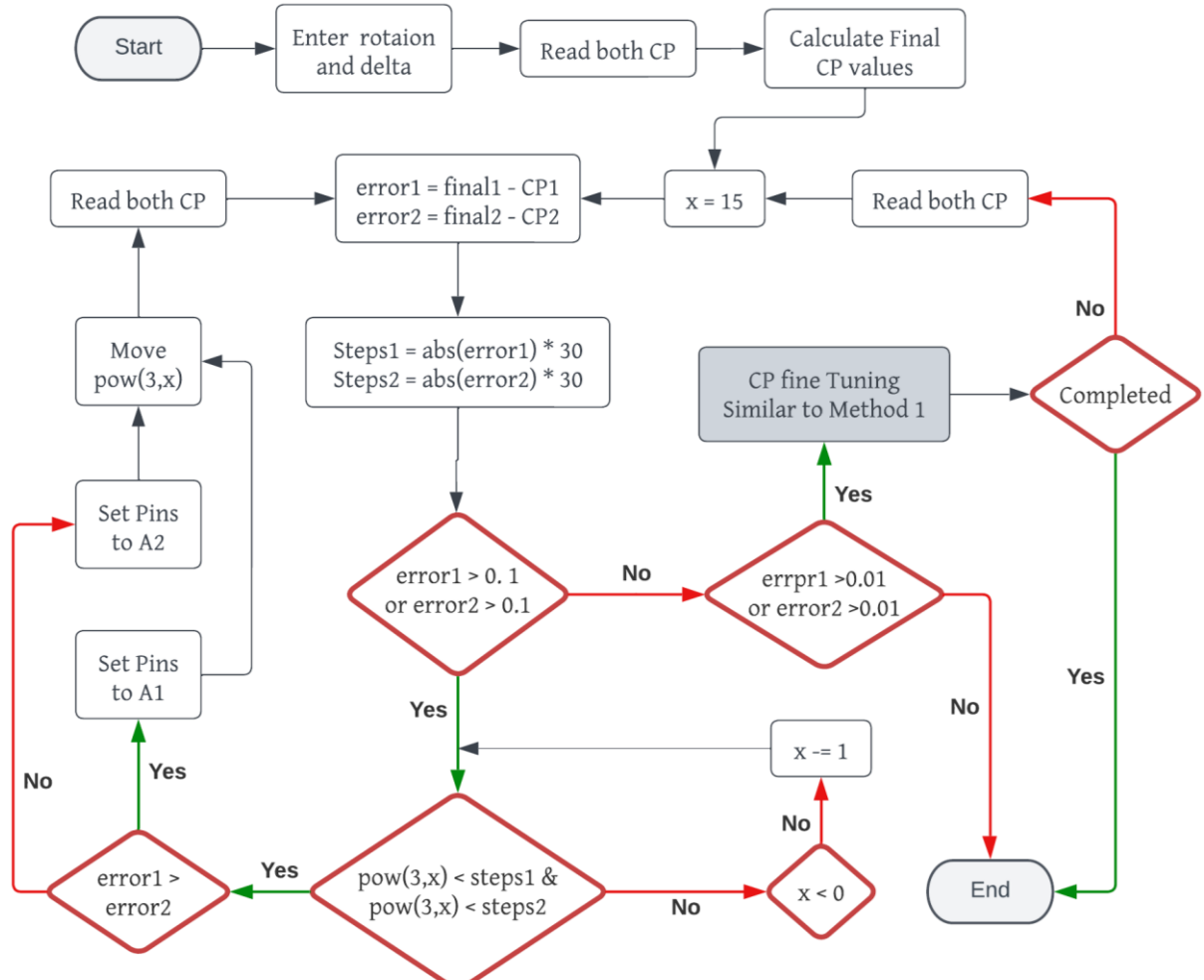


Figure 66 Bipod Dependent Hunting Algorithm

The experiments showed that the algorithm needed only 100-120 inputs of measurements to correct itself under 100 nm whereas the previous algorithm took 400 iterations. Only the coarse control method for this algorithm is different, the fine control works as the same way as the previous one reciprocating across a step range of 20. This method was finalized for the bipod control and in cases of testing the first method will be employed. A flowchart of the algorithm is given below. Similar to previous algorithm, critical test cases were evaluated and verified. The videos/gifs can be found in the softcopy of the report or the ppt which is bundled with this.

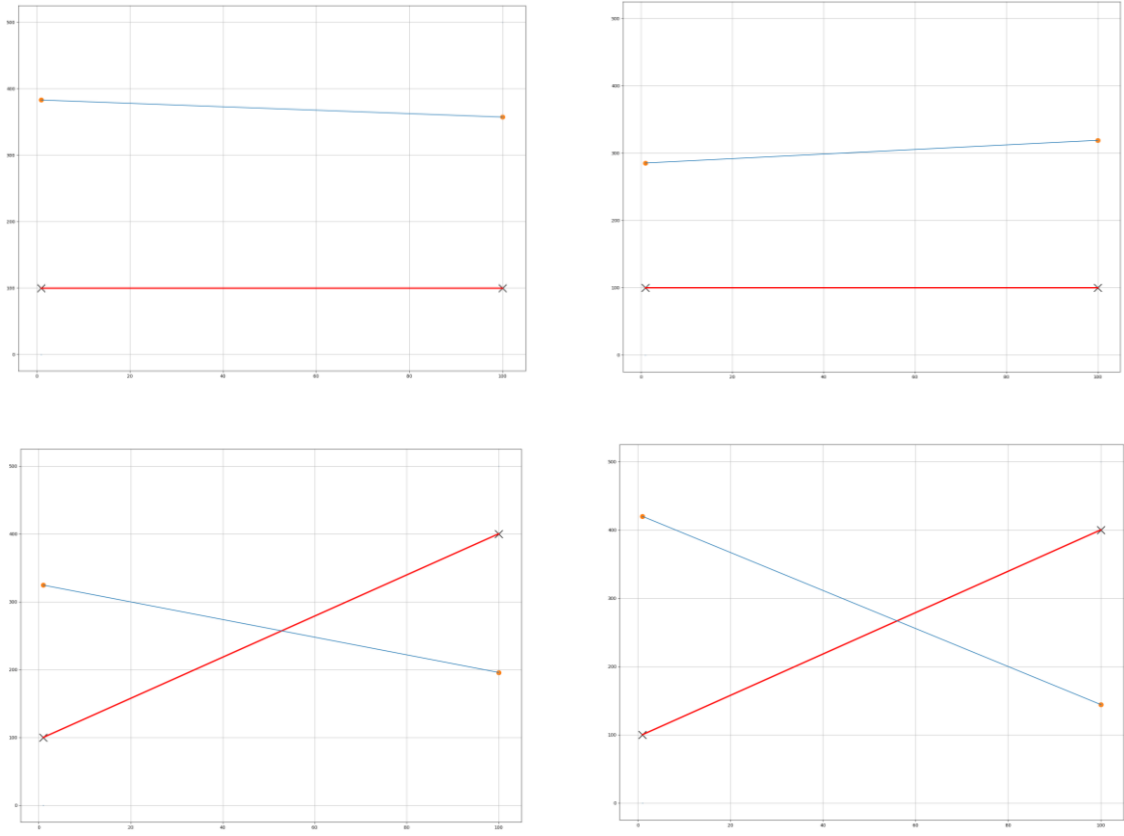


Figure 67 Test cases for Algorithm 2

7. Stewart Platform (Hexapod Assembly)

A Stewart platform consists of a fixed base and a movable platform connected by a series of six extendable and adjustable legs or kinematic chains. Each leg typically consists of a combination of linear actuators and universal joints that allow for both translational and rotational motion. The translational movement is provided by the Actuators connected in the Bipod assembly and the rotational stiffness can be given by the top and bottom flexures of the Actuators along with the connecting pad.

The basic principle of operation involves using the linear actuators to control the length of each leg. By adjusting the actuator lengths independently, the position and orientation of the movable platform can be precisely controlled in all six degrees of freedom (3 translations and 3 rotations). To determine the required actuator lengths for a desired position and orientation of the movable platform, a mathematical model based on the principles of kinematics is utilized. This model takes into account the geometric arrangement of the legs, the length of each leg, and the angles at the universal joints. The control system of a Stewart platform receives input commands specifying the desired position and orientation of the platform. These

commands are translated into the corresponding actuator lengths through an inverse kinematics algorithm. The control system then adjusts the actuators accordingly to achieve the desired configuration.

The real-time feedback from sensors, such as encoders or position sensors, is crucial for accurate control. These sensors provide information about the actual position and orientation of the movable platform, which is compared to the desired values. Any discrepancies are used to adjust the actuator lengths and bring the platform into alignment with the desired pose. Overall, the combination of precise actuator control, kinematic modelling, and real-time feedback enables the Stewart platform to provide accurate and multi-axial motion control. Its versatility and stability make it suitable for various applications where precise positioning and motion are required.

The model below shows a visualization of a simple hexapod. The yellow dots represent the free rotational joints substituted by flexures in our actuator and the link rods are replaced by our single actuator. The top movable plate is our mirror segment. The links are assembled at an angle of 15° in our Hexapod assembly.

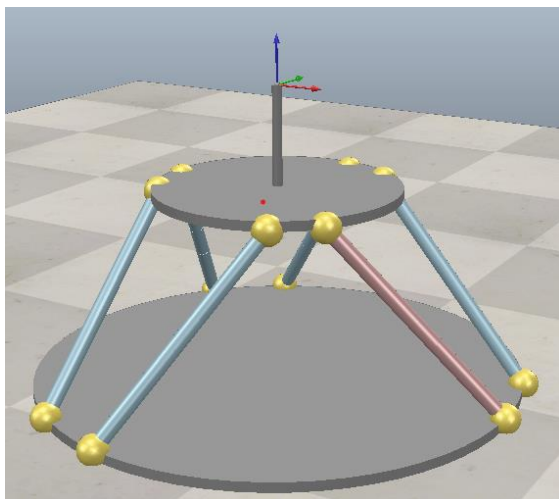


Figure 68 Static simulation model

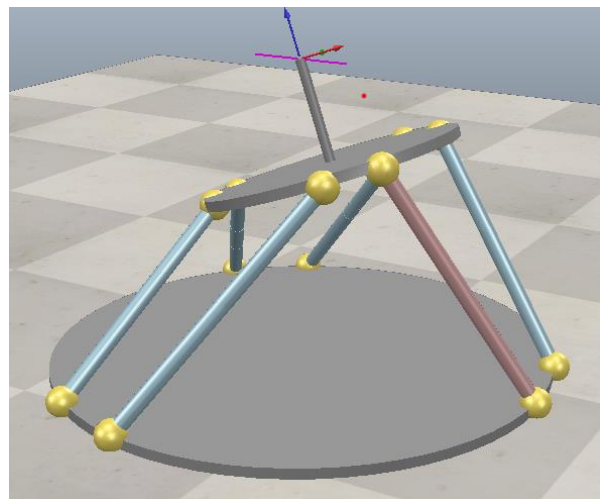


Figure 69 Movement of Hexapod in 6 DOF

7.1. Assembly of Hexapod

2 Hexapod support structures were designed by my colleagues: one for testing and one for final assembly into the Telescope. The 3 Bipods were thoroughly tested and put into proper positions. The assembly required proper measurements and dimensions that matched the designed hexapod. All the actuators were put to their 0 positions along with the LVDT sensors.

The Bipod pads were tested to be in-plane with the other 2. The 3 bipods mutually formed an angle of 120° with each other. The complete assembly of the bipods is shown below.

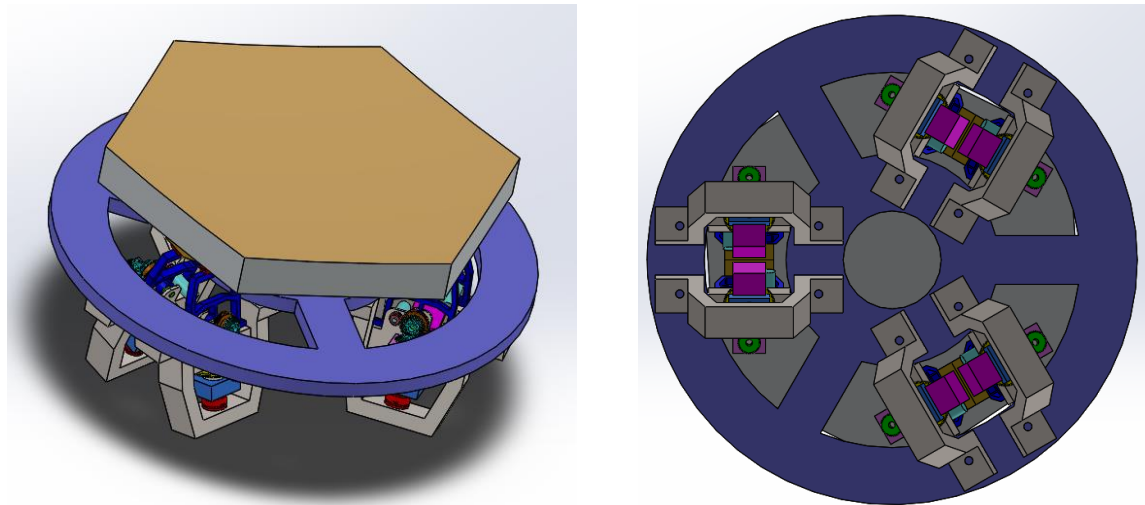


Figure 70 Hexapod Dummy model

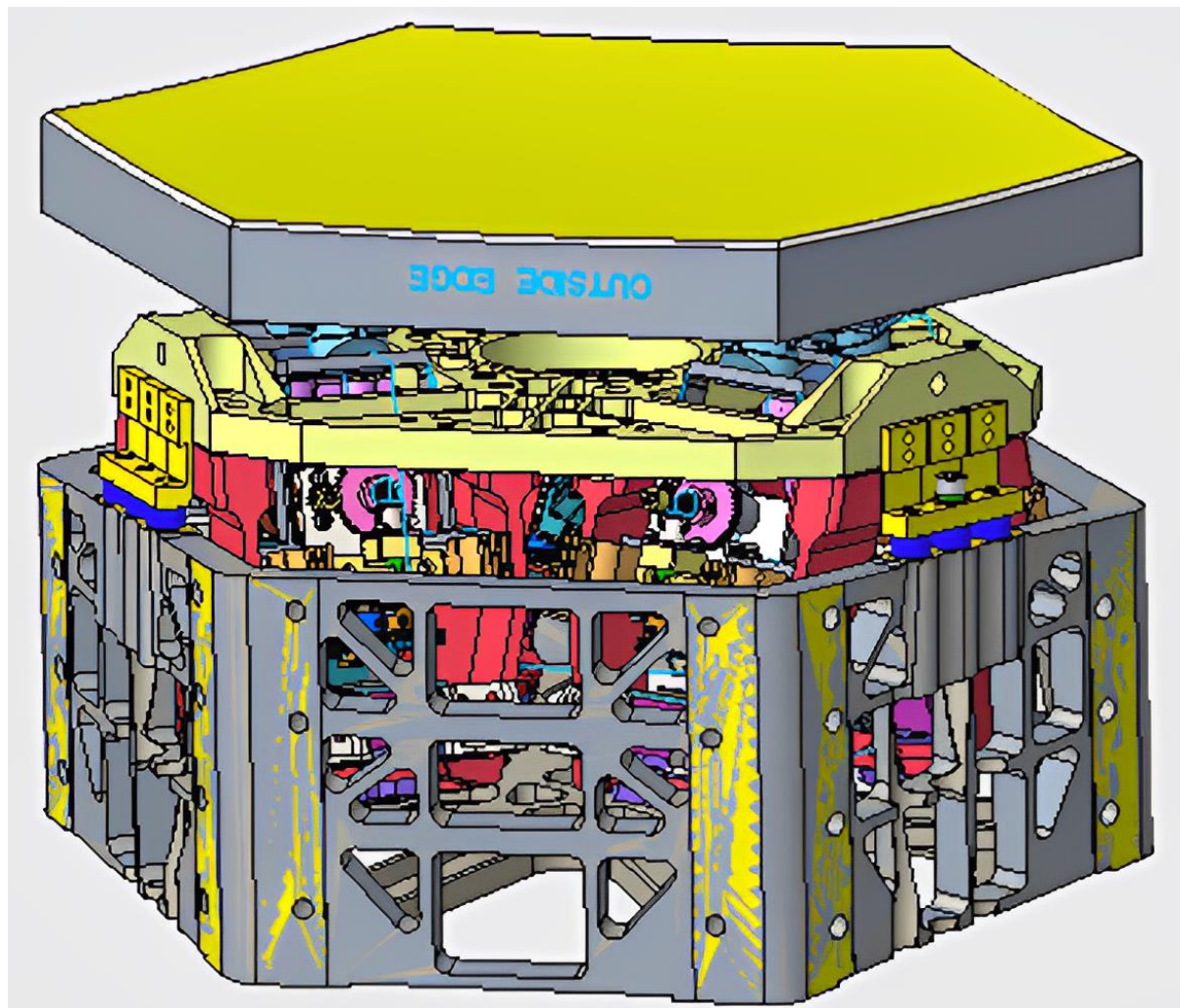


Figure 71 Hexapod final CAD model

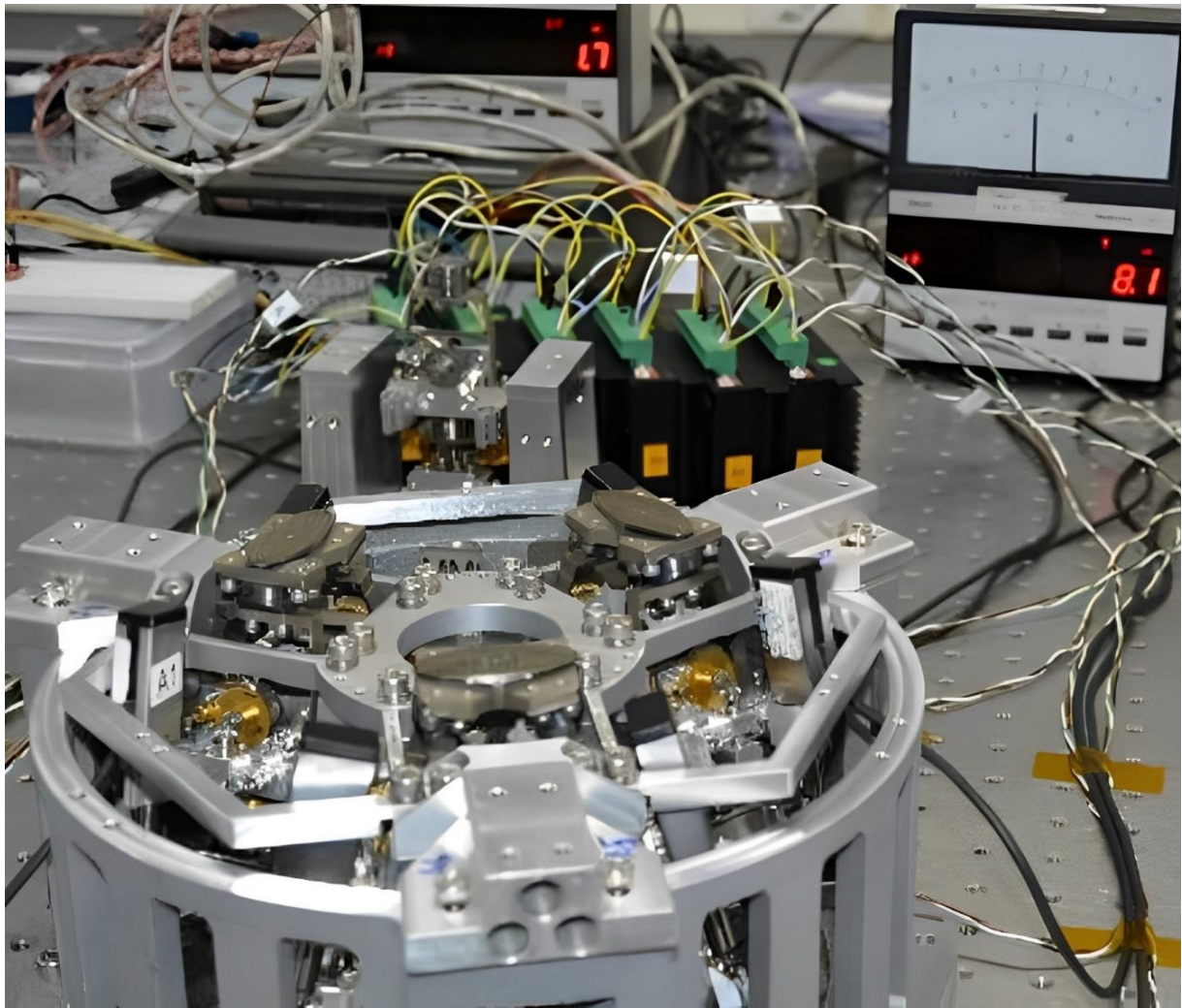


Figure 72 Hexapod test setup with Drive electronics

7.2. Inverse Kinematics of the Hexapod

Inverse kinematics of a hexapod refers to the process of determining the required actuator positions to achieve a desired position and orientation of the hexapod's platform (mirror in our case). In other words, it involves finding the link lengths that will result in a specific position and orientation of the mirror.

To perform inverse kinematics for a hexapod, a mathematical model of the hexapod's geometry and kinematic structure is used. This model includes the lengths of the Actuators and the position of the top and bottom points on the mirror segment and the base plate respectively. By applying trigonometry and geometric calculations, the inverse kinematics algorithm can solve for the joint angles that correspond to the desired position and orientation of the hexapod.

The inverse kinematics algorithm takes the desired coordinates and orientations of the end-effector as inputs. It then calculates the joint angles or actuator positions that will achieve these

desired values. This calculation involves solving a system of equations that relate the joint angles to the position and orientation of the hexapod.

The inverse kinematics of the hexapod uses rotation matrix to calculate the end positions on the plate and then vectors lengths are calculated before and after movement. The calculations for rotation matrix are given below.

$R_x(\alpha) = \begin{bmatrix} 1 & 0 & 0 \\ 0 & \cos \alpha & -\sin \alpha \\ 0 & \sin \alpha & \cos \alpha \end{bmatrix}$	$R_y(\beta) = \begin{bmatrix} \cos \beta & 0 & \sin \beta \\ 0 & 1 & 0 \\ -\sin \beta & 0 & \cos \beta \end{bmatrix}$	$R_z(\gamma) = \begin{bmatrix} \cos \gamma & -\sin \gamma & 0 \\ \sin \gamma & \cos \gamma & 0 \\ 0 & 0 & 1 \end{bmatrix}$
$R_x(\alpha)R_y(\beta)R_z(\gamma) = \begin{bmatrix} \cos \beta \cos \gamma & -\cos \beta \sin \gamma & \sin \beta \\ \cos \alpha \cos \gamma + \sin \alpha \sin \beta \cos \gamma & \cos \beta \cos \gamma - \sin \alpha \sin \beta \sin \gamma & -\sin \alpha \cos \beta \\ \sin \alpha \sin \gamma - \cos \alpha \sin \beta \cos \gamma & \sin \alpha \cos \gamma - \cos \alpha \sin \beta \sin \gamma & \cos \alpha \cos \beta \end{bmatrix}$		

Table 16 Rotation Matrix Calculation

Where α , β and γ denote the rotation of points about the x, y and z axis respectively. Say there are 6 points on the top of the mirror plate in the initial position - p_1, p_2, p_3, p_4, p_5 and p_6 . The points are then transformed and rotated as per the rotation matrix calculated. The new points are denoted by $p'_1, p'_2, p'_3, p'_4, p'_5$ and p'_6 . The vector difference of these 2 points give us the increase or decrease in the actuator lengths of the Hexapod legs. The magnitude of the vector then gives the exact distance to move to achieve the desired position. This length is fed to the Actuators and the Hexapod assembly is moved.

$p_1 = \begin{bmatrix} x_1 \\ y_1 \\ z_1 \end{bmatrix}$	$p_2 = \begin{bmatrix} x_2 \\ y_2 \\ z_2 \end{bmatrix}$	$p_3 = \begin{bmatrix} x_3 \\ y_3 \\ z_3 \end{bmatrix}$	$p_4 = \begin{bmatrix} x_4 \\ y_4 \\ z_4 \end{bmatrix}$	$p_5 = \begin{bmatrix} x_5 \\ y_5 \\ z_5 \end{bmatrix}$	$p_6 = \begin{bmatrix} x_6 \\ y_6 \\ z_6 \end{bmatrix}$
$p'_1 = p_1 R$ $= \begin{bmatrix} x'_1 \\ y'_1 \\ z'_1 \end{bmatrix}$	$p'_2 = p_2 R$ $= \begin{bmatrix} x'_2 \\ y'_2 \\ z'_2 \end{bmatrix}$	$p'_3 = p_3 R$ $= \begin{bmatrix} x'_3 \\ y'_3 \\ z'_3 \end{bmatrix}$	$p'_4 = p_4 R$ $= \begin{bmatrix} x'_4 \\ y'_4 \\ z'_4 \end{bmatrix}$	$p'_5 = p_5 R$ $= \begin{bmatrix} x'_5 \\ y'_5 \\ z'_5 \end{bmatrix}$	$p'_6 = p_6 R$ $= \begin{bmatrix} x'_6 \\ y'_6 \\ z'_6 \end{bmatrix}$
$L_1 = p'_1 - p_1$	$L_2 = p'_2 - p_2$	$L_3 = p'_3 - p_3$	$L_4 = p'_4 - p_4$	$L_5 = p'_5 - p_5$	$L_6 = p'_6 - p_6$

Table 17 Magnitude of Movement of Actuators

Due to the errors and inconsistencies discussed in the chapter x, it is hard to control the entire hexapod in an open loop fashion when using the inverse kinematics as IK assumes the exact

positional movement has taken place when prompted. In the prototype testing, we will be taking care of 3 degrees of freedom using 3 capacitance probes working in a closed feedback control. The inverse kinematics will be used to verify and compare the results obtained in the process.

7.3. Z-control of Hexapod platform.

The z control of the platform involves uniform movement of the mirror plate. It is easy to imagine that the parallel movement of all bipods at the same time will not work due to the sinusoidal wave generated as a result of difference of their MRS positions. A three-point plane mechanism was used to determine the position and orientation of the mirror plate. 3 sensors placed at the center of the 3 bipods dictate the translational motion

The test mirror plate has a very high surface finish resulting in a flat surface. Using the 3 measured values from the sensors, one can form a plane and find the inclinations about the xy, yz and zx planes resulting in calculation of three movements: z, Rx and Ry. The in-plane movements can be found by placing sensors beside the mirror plate checking the translation in x and y directions.

The algorithm for Z control is similar to the bipod control. The values are calculated for the 3 sensors and coarse and fine motions are operated repeatedly via hunting. It follows the notion that as the 3 points form a plane, and the mirror plate is also extremely flat, the 2 should overlap and coincide perfectly verifying the orientation of the mirror plate

7.4. Bonding of Dummy Mirror

3 blocks were developed as a type of location blocks that helps align the mirror w.r.t to hexapod assembly. The bonding material is space compatible which ensures very less evaporation of the binding material due to absence of pressure in space. The mirror was left to cure for 7 days along with a witness sample to compare or test the bond strength.

7.5. Rx and Ry control

These 2 rotations can be easily using the same setup from the previous test. Rotation matrix calculated in the previous topics can rotate the current measurements by the desired angles and give the new values to be read by the sensors to achieve the desired rotation. One thing to note here is that the rotation matrix also displaces the x and y coordinates of the sensors which in reality aren't displaced. To tackle this problem equation of plane needs to be formed using the transformed values. Inputting the values of the sensor's location in the xy plane gives the z

value of the target position that the sensors need to read for desired orientation. Using the control algorithm of z control is possible to control these as well.

8. Summary and Conclusion

The design and Development of a compact Actuator capable of dual movement was completed along with the control and assembly of bipod and hexapod systems. Parametric study and stress analysis of the Motion Reduction Flexure was performed calculating optimal reduction ratio for the desired range and resolution. Supporting parts were modelled and manufactured leading to the assembly of several actuators. Thorough QC of all the parts was done before starting the assembly due to sensitivity of the parts involved.

Control mechanism for the coarse and fine control of the Actuators was developed in Raspberry Pi using Thonny. Combined control for a given change of the actuator length was also developed. During the process, errors and inconsistencies between the internal and external sensors that affected the combined control of the actuator were reduced and an attempt to characterize the actuator was made. Due to mechanical errors and motor limitations, repeatability under 10 nm could not be achieved. The control method of the hexapod and bipod system was then changed to a active feedback control system.

The MRS designed for each actuator gave varied range and resolutions capping at 26 microns. The pairs for bipod assemblies were formed based on the closest values to minimize stresses and deviations when operating in closed loop. Control mechanism for the Bipod in 2 degrees of freedom was developed and successfully carried out reaching an angular resolution of 1 arc second and a translational resolution of 10 nm. The project then proceeded to assemble the complete hexapod and 3 degrees of freedom were controlled in the end.

8.1. Future work

The remaining 3 degrees of freedom needs to be controlled to achieve a complete hexapod mechanism. Although the Rz movement isn't necessary, it is still an objective of the project. The translational x and y movements can be controlled by placing sensors along the x and y axis. Although this method would still give the same results as when using inverse kinematics, a perfect inverse kinematics model for the hexapod platform is still the ideal method. The upcoming stages of the project will focus on controlling the remaining degrees of freedom and perfectly characterizing the actuator enabling it to operate via the IK solutions.

9. References

- [1] Gardner, Jonathan & Mather, John & Clampin, Mark & Doyon, Rene & Greenhouse, Matthew & Hammel, H. & Hutchings, John & Jakobsen, Peter & Lilly, Simon & Long, K. & Lunine, Jonathan & Mccaughrean, Mark & Mountain, Matt & Nella, John & Rieke, George & Rieke, Marcia & Rix, Hans-Walter & Smith, Eric & Sonneborn, George & Wright, Gillian. (2009). **The James Webb Space Telescope.** *Space Science Reviews.* 123. 485-606. 10.1007/s11214-006-8315-7.
- [2] Warden, Robert M. “**Cryogenic Nano-Actuator for JWST.**” (2012).
- [3] Gallagher, Benjamin & Smith, Koby & Knight, Scott & Sullivan, Joseph & Rudeen, Andrew & Babcock, Kevin & Hardy, Bruce & Barto, Allison & Wolf, Erin & Coppock, Eric & Davis, Clinton & Chonis, Taylor. (2018). **JWST mirror and actuator performance at cryo-vacuum.** 7. 10.1117/12.2312872.
- [4] R. Slusher, “**Motion Reducing Flexure Structure**”, US. Patent Number 5,969,892, Oct. 19, 1999.
- [5] Scott Streetman, Lana Kingsbury, “**Cryogenic Nano-positioner Development and Test for Space Applications**”, in IR Space Telescopes and Instruments, Proceedings of SPIE Vol. 4850, Sep. 2002.
- [6] Lana Kingsbury, Paul Atcheson, “**JWST Testbed Telescope**”, in Optical, Infrared and Millimeter Space Telescopes, Proceedings of SPIE Vol. 5487, June, 2004.
- [7] Feinberg, L. D., Clampin, M., Keski-Kuha, R., Atkinson, C., Texter, S., Bergeland, M., Gallagher, B. B. "James Webb Space Telescope optical telescope element mirror development history and results," Proc. SPIE 8442, Space Telescopes and Instrumentation 2012: Optical, Infrared, and Millimeter Wave, 84422B (2012).
- [8] Stahl, H. Philip, Lee D. Feinberg and Scott C. Texter, "IWST Primary Mirror Material Selection", SPill Vol.5487, p.818,2004.